Mapping exoplanetary ring systems using reflected light curves

Olivier Vos

Delft University of Technology

TU Delft

Mapping exoplanetary ring systems using reflected light curves

by

Olivier Vos

to obtain the degree of Bachelor of Science
at the Delft University of Technology,
to be defended publicly on Thursday August 22, 2024 at 11:00 AM.

Student number:	5617596	
Project duration:	February 26, 2024 – August 19, 2024	
Thesis committee:	Dr. P.M. Visser,	TU Delft, supervisor
	Dr. A.J.L. Adam,	TU Delft, supervisor
	Dr. K.P. Hart,	TU Delft
	Prof. Dr. S. Stallinga	TU Delft

Cover: Saturn's rings captured by NASA's Cassini spacecraft on Aug. 22, 2009. Credit: NASA/JPL-Caltech/Space Science Institute

TU Delft

Abstract

The next generation of telescopes will be able to directly measure the light curves of exoplanets. This thesis demonstrates the potential of using light curve analysis to study exoplanetary ring systems, with the goal of retrieving their albedo map and optical depth. This can improve our understanding of the composition, formation, and evolution of such systems. We construct a mathematical model that describes how light interacts with ring particles through absorption, transmission, and scattering. Applying this model to data of Saturn's rings from high-resolution images by NASA's Cassini space probe, albedo maps for the rings are constructed and the optical depth is found to be mostly consistent with existing literature. We then derive an analytic formula for the light curve of an exoplanetary ring system. This formula is converted into a numerical linear transformation that links the albedo map of a ring system to its light curve. Using the Moore-Penrose pseudoinverse and singular value decomposition this transformation is inverted, enabling the retrieval of the albedo map from the light curve. The method is tested using synthetic data of model ring systems while varying the axial tilt, observer direction, and signal-to-noise ratio from artificial Gaussian white noise. The results show that the method is generally effective at recovering the albedo map and optical depth for signal-to-noise ratios down to 10^3.

Contents

Symbols

Symbol	Quantity
(x, y, z)	Cartesian coordinates
$\hat{\mathbf{x}}, \hat{\mathbf{y}}, \hat{\mathbf{z}}$	Standard basis vectors
t	Time
r	Radius
D	Distance between star and observer
P	Star power
R	Orbital radius
ω	Orbital angular velocity
r_p	Planet radius
a	Inner ring radius
b	Outer ring radius
d	Ring thickness
β	Axial tilt
$\hat{\mathbf{n}}$	Planet spin axis
$\hat{\mathbf{i}}$	Unit vector from planet to star
$\hat{\mathbf{o}}$	Unit vector from planet to observer
$\hat{\mathbf{s}}$	Ring surface vector
$\mathcal{B}$	Backward scattering albedo map
$\mathcal{F}$	Forward scattering albedo map
$\mathcal{M}$	Arbitrary albedo map
$\mathcal{A}$	Absorption
$\mathcal{T}$	Unimpeded transmission
τ	Optical depth
μ	Attenuation coefficient
V	Visible part of the ring (to the observer)
I	Illuminated part of the ring
$\mathfrak{D}$	Visible and illuminated part of the ring
F	Light curve
S/N	Signal-to-noise ratio
RMSD	Root mean square deviation

Introduction

Exoplanet research aims to discover and analyse planets orbiting other stars than the Sun. One of the goals of this is to find signs of molecules in their atmospheres that could indicate extraterrestrial life. But while these planets are many light-years away, they can't only teach us about what is out there in the universe, but also about ourselves. For instance, studying young exoplanets could improve our understanding of how Earth and the other planets in the Solar System formed billions of years ago.

Exoplanets were first theorized to exist by Giordano Bruno back in the late 1500s, but it took over 400 years before the technology was developed that could confirm their existence. The first exoplanet was discovered in 1992 by Aleksander Wolszczan and Dale Frail using the radial velocity method [1]. Since then, over 5000 exoplanets have been discovered, see Fig. 1.1. The vast majority of these were found using indirect methods: not the exoplanet itself is observed, but some effect it has on the light of its parent star. For instance, periodic dips in the apparent brightness of a star can be measured if an orbiting planet passes in front of it. This is known as the transit method.

The main difficulty with direct exoplanet detection is the fact that the light emitted by stars is billions of times brighter than that emitted or reflected by orbiting exoplanets, so that they get lost in the star's glare. However, with the cutting edge technology of today, new telescopes are currently under construction that will make direct exoplanet detection more feasible. This includes both ground-based telescopes, such as the European Southern Observatory's Extremely Large Telescope (ELT) in Chile, as well as space telescopes, such as NASA's Roman Space Telescope. The currently operational James Webb Space Telescope also has direct exoplanet detection capabilities. These telescopes are equipped with stellar coronagraphs that block out the direct starlight so that exoplanets can be resolved. Nevertheless, due to the enormous distances involved, we will be limited to a resolution of just one pixel; only the total light intensity of the planet is measurable. It might seem that this makes it impossible to retrieve information about the surface features of the planet, like whether it has continents and oceans. However, this is not the case. One can use the fact that the total intensity is a time-dependent function. The portion of the planet surface that is both illuminated by the star and visible to us changes over the course of one orbit much like the phases of the moon do. Furthermore, different parts of the planet are illuminated at different times as it spins around its axis.

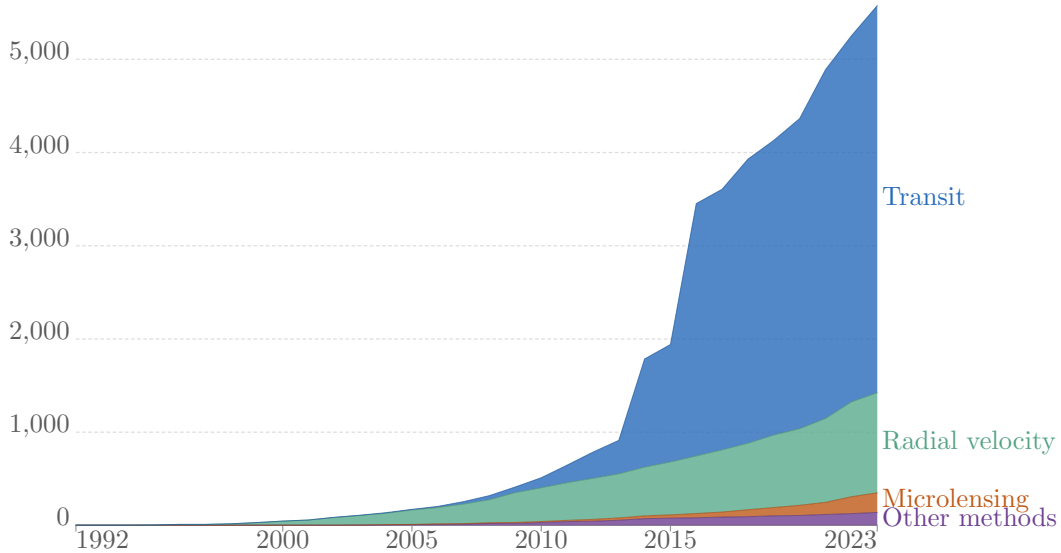

Figure 1.1: Cumulative number of exoplanets discovered, broken down by the method of identification: transit, radial velocity, microlensing, or other. [2]

This time-dependent signal is called the planet's light curve. Hidden in the light curve is information about the planet's surface. Multiple authors have studied the problem of retrieving the surface features of exoplanets based on mock observations of their light curve [3, 4, 5, 6, 7]. In this thesis we will apply a similar kind of analysis to study exoplanetary ring systems. So far, the rings of Saturn are the only substantial planetary ring system we know about. Detecting and mapping more of these structures will expand our knowledge about what types of ring systems exist in the universe and how common they are, as well as increase our understanding of the conditions under which they form, how they evolve over time, and how stable they are. First, in Ch. 2 we will create mathematical model for how light interacts with ring particles through absorption, transmission and scattering. In Sec. 2.2 we apply this model to analyse the rings of Saturn and retrieve their optical depth from data by NASA's Cassini space probe. Next, in Ch. 3 we derive an analytic expression for the light curve of an exoplanetary ring system. In Ch. 4 this formula will be converted into a numerical linear transformation that relates a ring system's albedo map, which determines what the rings looks like, to its light curve and vice versa. Finally, in Ch. 4.5 the developed theory will be applied to retrieve the albedo maps and optical depth of mock ring systems.

Optical properties of planetary rings

2.1 Model of the planetary ring system

2.1.1 Coordinate system, star, planet, observer, and rings

In this section we will precisely define our model and specify all relevant quantities and parameters within it. We use a Cartesian coordinate system (x, y, z) with the standard basis vectors $\hat{\mathbf{x}}$, $\hat{\mathbf{y}}$, and $\hat{\mathbf{z}}$. At the origin sits a star that is described as an isotropic point source, i.e., it radiates uniformly in all directions. It has a constant power P; this is the total amount of electromagnetic energy emitted per unit time. The star has a planet that orbits it in the xy-plane in a circle with radius R and angular frequency ω. The planet has an axial tilt angle β and spins around its axis $\hat{\mathbf{n}}$ with angular frequency Ω. We choose for $\hat{\mathbf{n}}$ to lie in the yz-plane, so that the planet's rotation axis is given by $\hat{\mathbf{n}} = \sin(\beta)\hat{\mathbf{y}} + \cos(\beta)\hat{\mathbf{z}}$. In reality rotating planets are slightly oblate due to centrifugal forces, for example the equatorial radius of Earth is about 0.3% larger than its polar radius, but we will neglect this effect and model the planet as a perfect sphere with radius r_p. At time $t = 0$ the planet is at $(-R, 0, 0)$ and we define a unit vector $\hat{\mathbf{i}}(t) = \cos(\omega t)\hat{\mathbf{x}} + \sin(\omega t)\hat{\mathbf{y}}$ that points from the planet to the star. We also define a unit vector $\hat{\mathbf{o}}$ that points from the planet to the observer. We assume the planet is far enough away from the observer that $\hat{\mathbf{o}}$ can be considered constant in time, with an azimuthal angle ϕ and a polar angle θ: $\hat{\mathbf{o}} = \cos(\phi)\sin(\theta)\hat{\mathbf{x}} + \sin(\phi)\sin(\theta)\hat{\mathbf{y}} + \cos(\theta)\hat{\mathbf{z}}$. Allowing for ω and Ω to be negative we can choose $\beta, \theta \in [0, \frac{\pi}{2}]$ without loss of generality. Equation (2.1) lists the three vectors defined thus far.

$$\hat{\mathbf{n}} = \begin{bmatrix} 0 \\ \sin\beta \\ \cos\beta \end{bmatrix}, \qquad \hat{\mathbf{i}}(t) = \begin{bmatrix} \cos\omega t \\ \sin\omega t \\ 0 \end{bmatrix}, \qquad \hat{\mathbf{o}} = \begin{bmatrix} \cos\phi\sin\theta \\ \sin\phi\sin\theta \\ \cos\theta \end{bmatrix} \tag{2.1}$$

The planet also has a ring system around it. This will be modeled as an annulus; the region between two concentric circles of radius a and b, with $r_p \leq a \leq b$, in the equatorial plane of the planet. The rotation axis of the rings is given by $\hat{\mathbf{n}}$, the same as the planet. Figure 2.1 shows schematic overview of the situation for the case $\hat{\mathbf{o}} = \hat{\mathbf{y}}$ and $\beta = 27°$ (the same tilt angle as Saturn's).

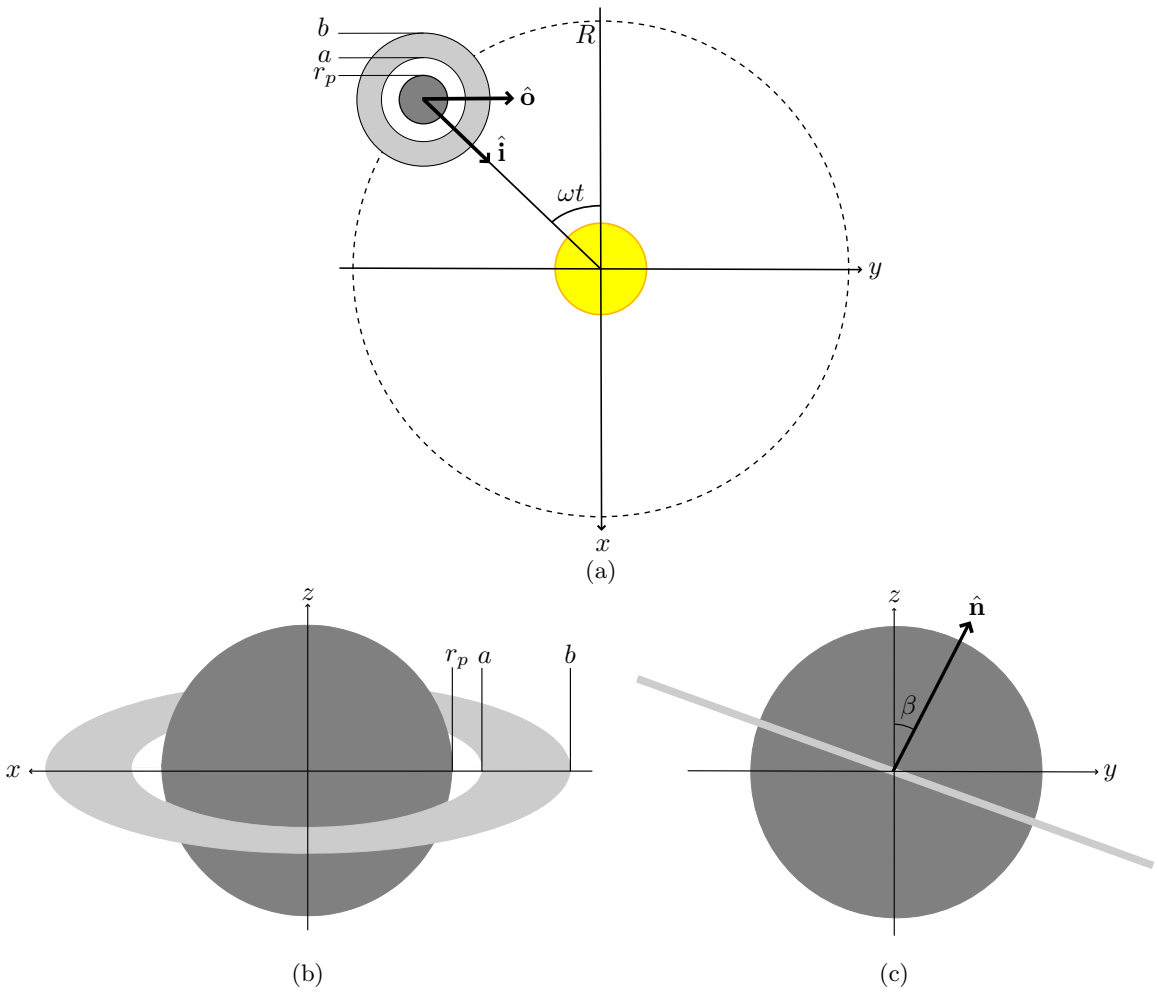

Figure 2.1: Schematic overview of the star, planet, and ring system for the case $\hat{\mathbf{o}} = \hat{\mathbf{y}}$ and $\beta = 27°$. The planet with radius r_p and inner and outer ring radius a and b respectively orbits the star, located at the origin, at a distance R with angular frequency ω in the xy-plane. The unit vectors $\hat{\mathbf{i}}$ and $\hat{\mathbf{o}}$ point from the planet to the star and observer respectively. The planet and ring system have the same tilt angle β and rotation axis $\hat{\mathbf{n}}$ which lies in the yz-plane. (a) Star, planet, and ring seen with a face-on view of the orbital plane. (b) Planet with ring seen from the $\hat{\mathbf{y}}$-direction. (c) Planet with the ring seen edge-on.

2.1.2 Ring albedo maps

A planetary ring system can be thought of as a region of space containing many separate pieces of material, called ring particles. When a photon from the star reaches the surface of a ring, we will say that one of three things can occur. First, it can simply pass straight through the ring without interacting with any of the particles within it. We will call this unimpeded transmission, and denote the fraction of the incident light that this happens to by $\mathcal{T}$. Second, the photon can be absorbed by a particle somewhere in the ring. We will denote this fraction this by $\mathcal{A}$. The third possibility is scattering: the photon can bounce off of any number of particles before exiting the ring system scattered in a random direction. We distinguish between to types of scattering: backward and forward scattering. Backward scattering, $\mathcal{B}$, means that the photon is scattered back into the same half-space adjacent to the ring system's surface that it came from. Forward scattering, $\mathcal{F}$, means that the photon is transmitted through the ring and scattered in a random direction out the other side. Figure 2.2 shows an illustration of all the possible interactions.

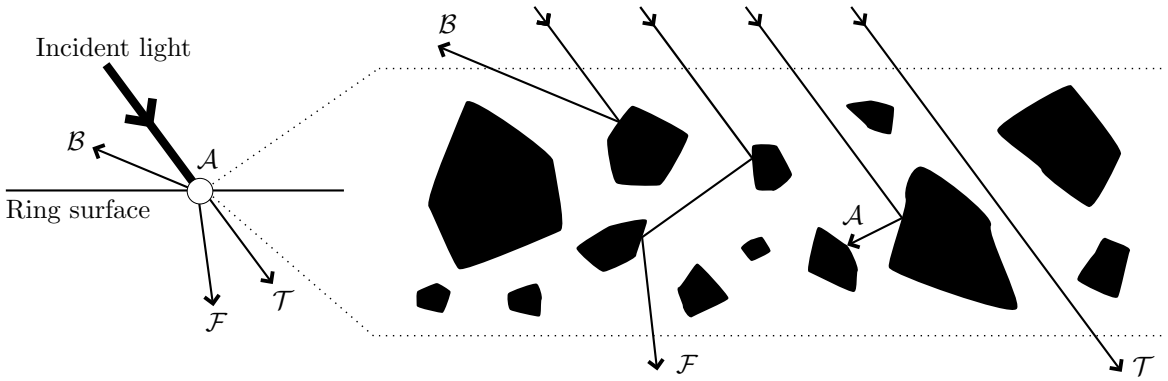

Figure 2.2: Illustration of the four ways in which incident light can interact with the ring system. The rings are a region of space containing many separate pieces of material. Photons can be scattered forward ($\mathcal{F}$) or backward ($\mathcal{B}$), be unimpededly transmitted ($\mathcal{T}$), or absorbed ($\mathcal{A}$).

The total energy must, of course, be conserved, so at every point on the ring surface the relation

$$\mathcal{B} + \mathcal{F} + \mathcal{A} + \mathcal{T} = 1 \tag{2.2}$$

must hold. We assume that the composition of the rings is radially symmetric, so that $\mathcal{B}$, $\mathcal{F}$, $\mathcal{A}$, and $\mathcal{T}$ only depend on the radial distance r along the ring system. We call $\mathcal{B}$ the backward scattering map. This also known as an albedo map. The albedo of a surface is defined as the fraction of incident light that is diffusely reflected back (as opposed to being absorbed). The map $\mathcal{B}$ assigns to each point on the ring system's surface a value from 0 to 1 indicating the fraction of the incident light that this happens to. Thus $\mathcal{B}$ determines the appearance of the ring system on the side that faces the star. Note that $\mathcal{B}$ is not the same as the albedo of the individual particles the rings are composed of, since light can also be transmitted through the rings and continue on at the other side, which is not considered in the usual definition of the albedo of a surface. Instead, $\mathcal{B}$ can be thought of as the effective albedo of the ring system as a whole; the pieces of material together with the empty spaces between them. Similarly, we call $\mathcal{F}$ the forward scattering map. This map determines what the rings look like on the side facing away from the star.

There are two main ways in which the two maps can be related to each other. The first is the thick ring approximation. This applies to rings that are thick and dense enough such that effectively no light just passes through them unimpeded: $\mathcal{T} = 0$. In this case the light that penetrates the rings to a certain depth drops off exponentially as this depth increases, so that $\mathcal{F} \ll \mathcal{B}$. The drop-off rate is determined by the optical depth $\tau(r)$ of the rings. The forward scattering map $\mathcal{F}$ is then related to the backward scattering map $\mathcal{B}$ according to

$$\mathcal{F}(r) = (1 - \mathcal{B}(r)) \cdot e^{-\tau(r)} \tag{2.3}$$

Assuming that the composition of the rings is homogeneous in the $\hat{\mathbf{n}}$-direction, the optical depth can be written as $\tau(r) = \mu(r)d(r)$, where d is the thickness of the ring and μ is called the attenuation coefficient, which depends on the wavelength of the incident light and the ring's composition. Generally a shorter wavelength and a denser material will result in a larger attenuation coefficient.

The other method of relating $\mathcal{B}$ and $\mathcal{F}$ is through the thin ring approximation. This is applicable when the rings are thin and sparse enough such that the majority of the incident light is unimpededly transmitted: $\mathcal{T} \approx 1$, and thus $\mathcal{B}, \mathcal{F}, \mathcal{A} \ll 1$. In this case the photons that are scattered forward encounter on average the same number of ring particles as the photons that are backscattered. This results in the probabilities for both types of scattering to be the same, so that the two albedo maps are related by

$$\mathcal{F}(r) = \mathcal{B}(r) \tag{2.4}$$

2.2 Optical depth retrieval of Saturn's rings using albedo maps

We will apply the theory of Sec. 2.1.2 to analyse the ring system of the only extensively ringed planet that real-world data exists for: Saturn. This will be done by creating a backward and forward scattering map of Saturn's rings based on high resolution images taken by NASA's Cassini space probe. These images are shown in Fig. 2.3. Figure 2.3a shows a slice of the illuminated side of the rings. This image has a resolution of 430 x 5776 pixels and will be used to construct the backward scattering map $\mathcal{B}(r)$. Figure 2.3b is a slice of the unilluminated side. It has a resolution of 1425 x 11795 pixels and will be used to construct the forward scattering map $\mathcal{F}(r)$. Saturn's ring system is often grouped into several sub-rings (A to F), and gaps in the rings are given names so they can be referred to. Our albedo maps will cover the C, B, and A rings; from the Colombo gap to the Keeler gap. The maps are made by taking a 5 pixel wide slice from both images, and then resizing these into 1 x 200 pixel images. For the vertical resizing, the average pixel value is taken, in order to counteract any noise in the images. The horizontal resizing is done so that the two maps can be lined up well. At each pixel, the value of the albedo is then defined as the sum of the RGB-values of the pixel, normalized so that the maximum possible albedo, corresponding to an RGB-value of (255,255,255), is 1. On physical grounds, the two maps must be normalized such that at every radius r along the rings we have that $\mathcal{B} \geq \mathcal{F}$ and $\mathcal{B} + \mathcal{F} \leq 1$. We do this by first dividing $\mathcal{F}(r)$ by $\max_r \left\{ \frac{\mathcal{F}(r)}{\mathcal{B}(r)} \right\}$, and subsequently dividing both $\mathcal{B}(r)$ and $\mathcal{F}(r)$ by $\max_r \{\mathcal{F}(r) + \mathcal{B}(r)\}$. Figure 2.4 shows the two scattering maps plotted together. Using Eq. (2.3) the optical depth $\tau(r)$ of the rings can now be calculated. This is shown in Fig. 2.5. The results are discussed in Sec. 5.1.

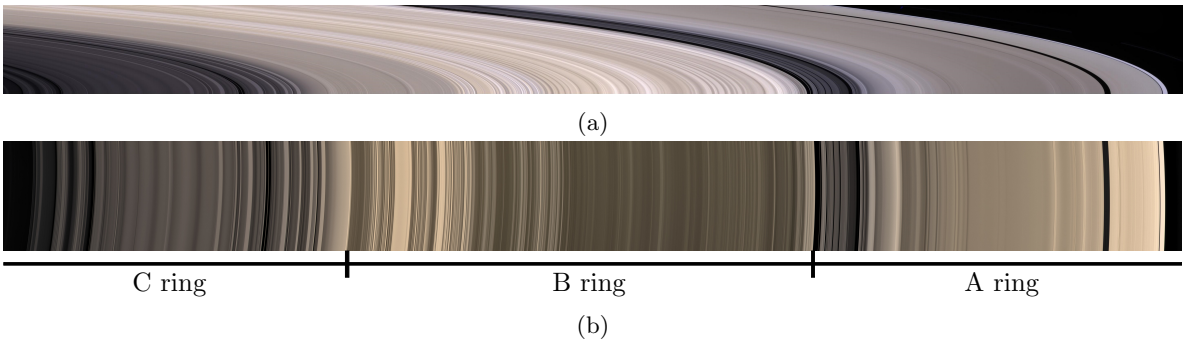

(a)

(b)

Figure 2.3: High resolution images of slices of Saturn's C, B, and A rings, taken by NASA's Cassini space probe. (a) Illuminated side, resolution: 430 x 5776 pixels [8]. (b) Unilluminated side, resolution: 1425 x 11795 pixels. [9]

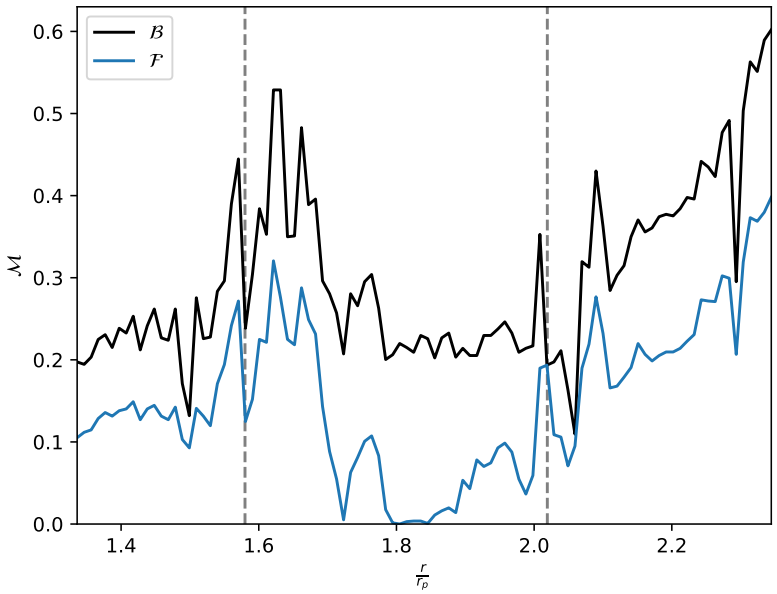

Figure 2.4: Backward scattering map $\mathcal{B}(r)$ and forward scattering map $\mathcal{F}(r)$ of the C, B and A rings of Saturn, constructed from high resolution images (Fig. 2.3) taken by NASA's Cassini space probe. The dotted lines indicate the boundaries between the three sub-rings. Due to the normalization that was applied we see that at the boundary between the B and A rings $\mathcal{B} = \mathcal{F}$ exactly, and that at the right end of the plot $\mathcal{B} + \mathcal{F} = 1$ exactly.

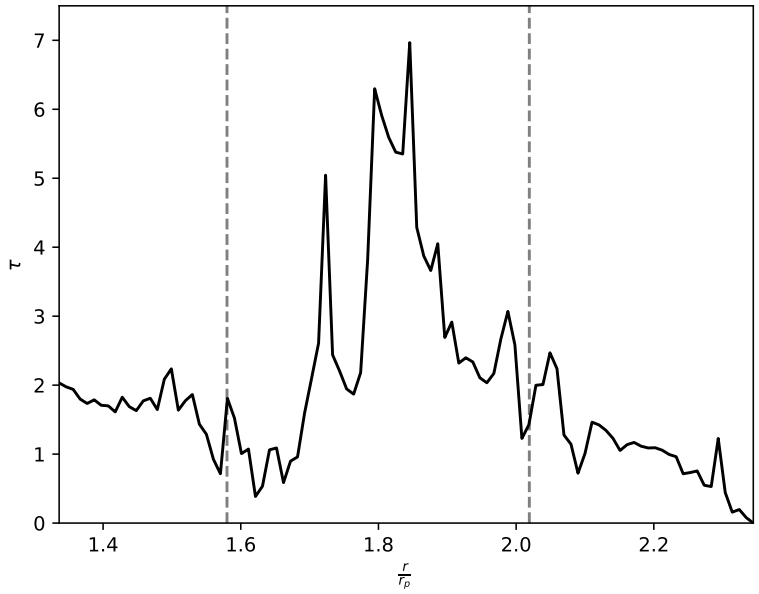

Figure 2.5: Optical depth $\tau(r)$ of the C, B, and A rings of Saturn, based on the scattering maps from Fig. 2.4. The dotted lines indicate the boundaries between the three sub-rings. For the C ring, where the thick ring approximation (Eq. (2.3)) from which τ is calculated is not accurate, the results, as expected, do not agree with the literature. For the B ring, where the thick ring approximation is very accurate, the values agree the literature. For the A ring, where the thick ring approximation is slightly accurate, the values agree somewhat with the literature.

Analytic expression for the light curve

In this chapter we will derive an analytic expression for the light curve of a planetary ring system. This is the total intensity of the light emitted by the star that scatters off the ring and is then detected by the observer as a function of time. It will be denoted as $F(t)$. In words, the formula for the light curve is as follows:

$$\begin{aligned} F(t) = &\text{ total power of the star} \\ &\times \text{ fraction of the total power that reaches the ring} \\ &\times \text{ fraction of incident light that is scattered off the ring} \\ &\times \text{ fraction of the scattered light that reaches the aperture of the telescope} \end{aligned} \tag{3.1}$$

3.1 Light curve of a surface element

We will first put this expression into mathematical terms for a surface element $d^2\hat{\mathbf{s}}$ of the ring. The total power of the star is P, so the star's intensity at the planet and ring, a distance R away, is $\frac{P}{4\pi R^2}$. The power that reaches the surface element $d^2\hat{\mathbf{s}}$ is then $\frac{P}{4\pi R^2} \cdot |\hat{\mathbf{n}} \cdot \hat{\mathbf{i}}| d^2\hat{\mathbf{s}}$, since $|\hat{\mathbf{n}} \cdot \hat{\mathbf{i}}| d^2\hat{\mathbf{s}}$ is the component of $d^2\hat{\mathbf{s}}$ that faces the star. The fraction of incident light that is scattered off the ring element is determined by the albedo maps $\mathcal{B}$ and $\mathcal{F}$ of the rings. At any point of the planet's orbit there is both backward and forward scattering occurring, but light can only reach the observer in one of these two ways. Using the visual intuition provided by Fig. 2.1 we see that if $\omega(\hat{\mathbf{n}} \cdot \hat{\mathbf{o}}) > 0$ the backward scattered light can reach the observer in the first half of the planet's orbit ($0 < \omega t < \pi$), and the forward scattered light can reach the observer in the second half of the orbit ($\pi < \omega t < 2\pi$). If $\omega(\hat{\mathbf{n}} \cdot \hat{\mathbf{o}}) < 0$ it is the opposite. Since $\mathcal{B}$ and $\mathcal{F}$ are generally different maps, this means that the task of retrieving the albedo of the rings from their light curve must actually be split into two instances of the same type of problem: retrieving the backward scattering map $\mathcal{B}$ from the light curve of one half of the orbit, and retrieving the forward scattering map $\mathcal{F}$ from the other half. Of course the absorbed light can never reach the observer. The same goes for the unimpededly transmitted light, although the observant reader might point out that technically this light would reach the observer if $\hat{\mathbf{o}}$ lies in the xy-plane and when $\hat{\mathbf{i}}(t) \parallel \hat{\mathbf{o}}$ and $\hat{\mathbf{i}}(t) \cdot \hat{\mathbf{o}} = -1$. We will however ignore this special case, which is discussed in more detail at the end of Sec. 3.2. The scattered light that can reach the observer spreads throughout a half-space adjacent to the surface of the ring system. Thus, the intensity detected by the observer is found by multiplying by $\frac{1}{2\pi D^2}$, with D the distance between the observer and the star, and finally by $|\hat{\mathbf{n}} \cdot \hat{\mathbf{o}}|$, the fraction of the surface element that is directed towards the observer. Putting all this together we find that the contribution dF of the surface element $d^2\hat{\mathbf{s}}$ to the total light curve is given by Eq. (3.2), where $\mathcal{M}(\hat{\mathbf{s}})$ is the appropriate albedo map, at the surface element $d^2\hat{\mathbf{s}}$. We have also divided by $\frac{P}{4\pi D^2}$, the observed intensity of the starlight, since astronomers usually measure the intensity of the signal of interest relative to the star's intensity instead of the absolute intensity. [10]

$$dF = \frac{|\hat{\mathbf{n}} \cdot \hat{\mathbf{o}}|}{2\pi R^2} |\hat{\mathbf{n}} \cdot \hat{\mathbf{i}}| \mathcal{M}(\hat{\mathbf{s}}) d^2\hat{\mathbf{s}} \tag{3.2}$$

3.2 Shadowing and blocking effects of the planet

To arrive at the total light curve Eq. (3.2) should not be integrated over the whole ring, but only over the part that is both illuminated by the star and visible to the observer. Indeed at any time there is some part of the ring that is not illuminated by the star because the planet is positioned in between the star and that part of the ring. In other words, part of the ring is shadowed by the planet. This part does not contribute to the light curve. Another part of the ring is also blocked from the view of the observer because the planet is in the way, even if that part is illuminated by the star. We will

call the visible and illuminated part of the ring $\mathfrak{D}(t)$. The total light curve is then given by Eq. (3.3), where we used Eq. (2.1) to work out $|\hat{\mathbf{n}} \cdot \hat{\mathbf{i}}| = \sin\beta|\sin\omega t|$.

$$F(t) = \frac{|\hat{\mathbf{n}} \cdot \hat{\mathbf{o}}|}{2\pi R^2} \sin\beta|\sin\omega t| \iint\limits_{\mathfrak{D}(t)} \mathcal{M}(\hat{\mathbf{s}}) d^2\hat{\mathbf{s}} \tag{3.3}$$

Now we must find out what exactly the region $\mathfrak{D}(t)$ is. If we call the illuminated part of the ring $I(t)$ and the part visible to the observer V, then $\mathfrak{D}(t)$ is then given by

$$\mathfrak{D}(t) = I(t) \cap V. \tag{3.4}$$

We assume that the orbital radius R is large enough such that the light rays from the star essentially travel in parallel. This way, the planet creates an infinitely long, perfectly cylindrical region of space behind it that is not illuminated by the star. This way there are no places that can be reached by some of the light but not by all, which would result in a transition region between fully lit and fully dark areas. Instead there is a sharp division between the illuminated and shadowed regions. The shadowed section of the ring is then exactly that part of it which intersects with the cylindrical region of space behind the planet. To find out what this section is, we will define the ring by set of points in a Cartesian coordinate system (a different one than the one in which the model is defined in Sec. 2.1) and rotate the system such that when viewed from the $\hat{\mathbf{x}}$ direction in this coordinate system (with $\hat{\mathbf{z}}$ facing upwards) it looks the same as when looking at it from the star. We start by defining the ring system as

$$S = \left\{ \begin{bmatrix} x \\ y \\ 0 \end{bmatrix} : a \leq \sqrt{x^2 + y^2} \leq b \right\}. \tag{3.5}$$

We can rotate the ring in three-dimensional space by multiplying each point by a rotation matrix $R_{\hat{\mathbf{u}},\theta}$ given by Eq. (3.6), which rotates points around the unit axis $\hat{\mathbf{u}} = (u_x, u_y, u_z)$ by θ radians [11]. We define the multiplication of a set of vectors S by a matrix R according to Eq. (3.7).

$$R_{\hat{\mathbf{u}},\theta} = \begin{bmatrix} \cos\theta + u_x^2(1-\cos\theta) & u_x u_y(1-\cos\theta) - u_z\sin\theta & u_x u_z(1-\cos\theta) + u_y\sin\theta \\ u_y u_x(1-\cos\theta) + u_z\sin\theta & \cos\theta + u_y^2(1-\cos\theta) & u_y u_z(1-\cos\theta) - u_x\sin\theta \\ u_z u_x(1-\cos\theta) - u_y\sin\theta & u_z u_y(1-\cos\theta) + u_x\sin\theta & \cos\theta + u_z^2(1-\cos\theta) \end{bmatrix} \tag{3.6}$$

$$R \cdot S := \{R \cdot s : s \in S\} \tag{3.7}$$

First we rotate the ring around the x-axis by $-\beta$, the negative of the tilt angle. The result is S_β, see Eq. (3.8). This way the ring's orientation in this coordinate system matches its actual physical orientation in the coordinate system of the model.

$$S_\beta = R_{\hat{\mathbf{x}},-\beta} \cdot S = \left\{ \begin{bmatrix} x \\ y\cos\beta \\ -y\sin\beta \end{bmatrix} : a \leq \sqrt{x^2 + y^2} \leq b \right\} \tag{3.8}$$

Now S_β must be rotated such that when viewed from the $\hat{\mathbf{x}}$ direction it looks the same as when looking at it from the star, i.e. looking from the $\hat{\mathbf{i}}$ direction. This means we need to rotate around the z-axis by $-\omega t$ radians. The result $S_i(t)$ is given by Eq. (3.9).

$$S_i(t) = R_{\hat{\mathbf{z}},-\omega t} \cdot S_\beta = \left\{ \begin{bmatrix} x\cos\omega t + y\cos\beta\sin\omega t \\ -x\sin\omega t + y\cos\beta\cos\omega t \\ -y\sin\beta \end{bmatrix} : a \leq \sqrt{x^2 + y^2} \leq b \right\} \tag{3.9}$$

Using $S_i(t)$ we can easily determine the illuminated part of the ring at time t. For $s \in S$ let $s_i = (s_{i_1}, s_{i_2}, s_{i_3})$ be the corresponding point in S_i according to $s_i = R_{\hat{\mathbf{z}},-\omega t} R_{\hat{\mathbf{x}},-\beta} \cdot s$. If we imagine the planet with radius r_p being centered at the origin, the point on the ring represented by s is certainly illuminated if it is in front of the planet, i.e. if $s_{i_1} > 0$. If $s_{i_1} < 0$, it is only illuminated if at that point the ring extends out sideways beyond the edge of the planet, so if $\sqrt{s_{i_2}^2 + s_{i_3}^2} > r_p$. Thus the illuminated section of the ring is given by

$$I(t) = \left\{ s \in S : s_{i_1} > 0 \vee \sqrt{s_{i_2}^2 + s_{i_3}^2} > r_p \right\}. \tag{3.10}$$

Now we will determine the part of the ring that is visible to the observer. To do this we rotate the ring from its actual physical orientation in the model, which corresponds to S_β, to its orientation as seen by the observer, looking from the $\hat{\mathbf{o}}$ direction. The axis $\hat{\boldsymbol{\xi}}$ for this rotation is perpendicular to both $\hat{\mathbf{x}}$ and $\hat{\mathbf{o}}$, and the rotation angle ζ is (minus) the angle between $\hat{\mathbf{x}}$ and $\hat{\mathbf{o}}$, which can be found using the inner product formula $\hat{\mathbf{x}} \cdot \hat{\mathbf{o}} = |\hat{\mathbf{x}}||\hat{\mathbf{o}}| \cos\zeta = \cos\zeta$. Thus $\hat{\boldsymbol{\xi}}$ and ζ are given by Eq. (3.11). The result S_o is given by Eq. (3.12). In the special case that $\hat{\mathbf{x}}$ is parallel to $\hat{\mathbf{o}}$ the denominator in Eq. (3.11) is zero, so the formula does not work. In this case we must do nothing if $\hat{\mathbf{x}} \cdot \hat{\mathbf{o}} = 1$ and rotate by π around the z-axis if $\hat{\mathbf{x}} \cdot \hat{\mathbf{o}} = -1$.

$$\hat{\boldsymbol{\xi}} = \frac{\hat{\mathbf{x}} \times \hat{\mathbf{o}}}{|\hat{\mathbf{x}} \times \hat{\mathbf{o}}|}, \qquad \zeta = -\arccos(\hat{\mathbf{x}} \cdot \hat{\mathbf{o}}) \tag{3.11}$$

$$S_o = R_{\hat{\boldsymbol{\xi}},\zeta} \cdot S_\beta. \tag{3.12}$$

The part V of the ring that is visible to the observer is determined using S_o exactly the same way as how the illuminated part $I(t)$ was determined using $S_s(t)$. For $s \in S$ we let $s_o = (s_{o_1}, s_{o_2}, s_{o_3})$ be the corresponding point in S_o according to $s_o = R_{\hat{\boldsymbol{\xi}},\zeta} R_{\hat{\mathbf{x}},-\beta} \cdot s$. V is then given by

$$V = \left\{ s \in S : s_{o_1} > 0 \vee \sqrt{s_{o_2}^2 + s_{o_3}^2} > r_p \right\}, \tag{3.13}$$

and using Eq. (3.4) we finally find that the visible and illuminated part of the ring as a function of time is given by

$$\mathcal{D}(t) = \left\{ s \in S : \left(s_{i_1} > 0 \vee \sqrt{s_{i_2}^2 + s_{i_3}^2} > r_p \right) \wedge \left(s_{o_1} > 0 \vee \sqrt{s_{o_2}^2 + s_{o_3}^2} > r_p \right) \right\}. \tag{3.14}$$

Note that while determining V we ignored any effects due to the star blocking the planet and ring from view if they were to move behind the star from the perspective of the observer. In reality these effects would occur for a small part of the orbit if $\hat{\mathbf{o}}$ lies approximately in the xy-plane. A bigger problem than this blocking, however, is that in this situation the planet and rings get so close to the star from the observer's point of view that light coming directly from the star cannot be properly blocked by a coronagraph anymore. This light would thus reach the observing telescope and ruin its measurements of the light curve of the planetary ring system because the direct star light is billions of times brighter. Since this happens only in rare cases and for short parts of the planet's orbit we will ignore these effects by assuming that the star has no physical dimensions and that no star light reaches the observer directly (as we already did in Secs 2.1.1) and 2.1.2 respectively). For some examples of what light curves generated using this model look like, see Sec. 4.2.

Retrieval of the ring albedo map

In the previous chapter an analytic expression for the light curve $F(t)$ of a planetary ring system given its albedo maps $\mathcal{B}$ and $\mathcal{F}$ was derived. This chapter will be dedicated to solving the inverse problem: retrieving the albedo maps given the light curve. We will also analyse these results to retrieve the optical depth $\tau(r)$ by applying the thick ring approximation, Eq. (2.3).

4.1 Numerical expression for the light curve

Retrieving the albedo map from the light curve cannot be done analytically, but there are numerical possibilities. We begin by dividing Eq. (3.3) by the factor in front of the integral. We will call the integral that remains $f(t)$:

$$f(t) = \iint\limits_{\mathbb{D}(t)} \mathcal{M}(\hat{\mathbf{s}}) d^2\hat{\mathbf{s}}. \tag{4.1}$$

Because, by assumption, $\mathcal{M}$ is radially symmetric, the light curve of a planetary ring system can be thought of as a linear combination of the light curves of individual circles with radii $a \leq r \leq b$, with the weights given by $\mathcal{M}(r)$. In this vein Eq. (4.1) can be rewritten as Eq. (4.2), where $A(r,t)$ is the contribution to $f(t)$ of a single circle with radius r and an albedo of 1.

$$f(t) = \int_a^b A(r,t)\mathcal{M}(r) dr \tag{4.2}$$

Written in this form, the problem can be easily discretized in space and time. This is done according to Eq. (4.3). Time is discretized into N_t equidistant points, either in the interval $\left[0, \frac{T}{2}\right]$ or $\left[\frac{T}{2}, T\right]$, with $T = 2\pi/\omega$ the length of one orbital period, depending on whether we are dealing with the first or the second half (see Sec. 3.1). Points on the ring S (see Eq. (3.5)) are described by an $N_r \times N_\phi$ sized grid of equidistant points on $[r_p, 2.44 \cdot r_p] \times [0, 2\pi\frac{N_\phi - 1}{N_\phi}]$ according to $(x, y, 0) = (r\cos\phi, r\sin\phi, 0)$.

$$\begin{aligned}
t_n &= \begin{cases} \frac{T}{2} \cdot \frac{n}{N_t - 1}, & \text{if } t \in \left[0, \frac{T}{2}\right] \\ \frac{T}{2} \cdot \frac{n}{N_t - 1} + \frac{T}{2}, & \text{if } t \in \left[\frac{T}{2}, T\right] \end{cases} && n \in \{0, \ldots, N_t - 1\} \\
r_n &= r_p \left(1 + 1.44 \cdot \frac{n}{N_r - 1}\right), && n \in \{0, \ldots, N_r - 1\} \\
\phi_n &= 2\pi \cdot \frac{n}{N_\phi}, && n \in \{0, \ldots, N_\phi - 1\}
\end{aligned} \tag{4.3}$$

Since the size of the ring system is not known in advance, some bounds must be chosen. The lower bound for the inner ring radius a is taken to be r_p because theoretically the ring system can start right at the planet's surface. The factor 2.44 in the upper bound for the outer ring radius b comes from an approximate solution for the Roche limit r_{Roche} given by Eq. (4.4) [12], where ρ_p and ρ_r are the densities of the planet and ring material respectively, which we assumed to be equal. The Roche limit is the distance from a planet within which an orbiting body tends to disperse and form rings due to the planet's tidal forces on it exceeding its self-gravitation. Outside of the Roche limit orbiting material tends to coalesce and ring systems are not likely to be found.

$$r_{\text{Roche}} = 2.44 r_p \left(\frac{\rho_p}{\rho_r}\right)^{1/3} \tag{4.4}$$

Applying the discretization to Eq. (4.2) results in an equation that may be written in the form

$$\mathbf{f} = \mathbf{A} \cdot \mathbf{M}. \tag{4.5}$$

$f(t)$ has become a vector $\mathbf{f} \in \mathbb{R}^{N_t}$ and $\mathcal{M}(r)$ is now a vector $\mathbf{M} \in \mathbb{R}^{N_r}$ according to

$$\mathbf{f} = [f(t_0), \ldots, f(t_{N_t-1})]^T, \qquad \mathbf{M} = [\mathcal{M}(r_0), \ldots, \mathcal{M}(r_{N_r-1})]^T \tag{4.6}$$

$\mathbf{A} \in \mathbb{R}^{N_t \times N_r}$ is a transformation matrix that depends on the geometry of the system, specifically on the parameters β and $\hat{\mathbf{o}}$. From Eq. (4.2) it follows that the components $\mathbf{A}_{ij}$ of $\mathbf{A}$ are given by

$$\begin{aligned} \mathbf{A}_{ij} = \sum_{n=0}^{N_\phi - 1} \mathbb{1}_{\mathcal{D}(t_i)}(s) \cdot r_j dr d\phi, \qquad & s = (r_j \cos\phi_n, r_j \sin\phi_n, 0), \\ dr = \frac{1.44 \cdot r_p}{N_r - 1}, \qquad & d\phi = \frac{2\pi}{N_\phi}. \end{aligned} \tag{4.7}$$

Determination of unknown parameters

The equation for the light curve (Eq. (3.3)) has in front of the integral a prefactor containing a number of different parameters. At the start of Sec. 4.1 we got rid of this prefactor on the way to deriving a numerical expression for the light curve. However, the values of all these parameters do need to be known if the ring albedo map is to be retrieved in practice. Here we briefly explain how these parameters can indeed be known. First, the distance D between the observer and the star as well as the orbital period of the exoplanet can be discovered using the stellar parallax method [13]. The star power P can then be derived from this distance combined measurements of the star's apparent brightness [14]. The parameters required to uniquely specify the planet's orbit, also known as the orbital elements, can be found using Doppler spectroscopy [15]. This way, the radius R of the planet's orbit as well as the orientation of the orbital plane, which determines our observer direction vector $\hat{\mathbf{o}}$, can be known. Lastly, the determination of the axial tilt angle β of the planet and rings, and consequently their rotation axis $\hat{\mathbf{n}}$ (see Eq. (2.1)) can be accomplished by applying a minimization process over $\beta \in [0, \pi/2]$ to the light curve (see Sec. 4.2) to find the best fitting value [7].

4.2 Examples of light curves

Before we proceed to actually retrieving ring albedo maps form the light curve, we will briefly touch upon what the light curve of an exoplanetary ring system looks like exactly. Figure 4.1 shows three examples. Both the integral $f(t)$ from Eq. (4.1) and the corresponding light curve $\widetilde{F}(t) = |\sin(\omega t)| \cdot f(t)$ are shown. $\widetilde{F}$ is proportional to the measured signal F from Eq. (3.3). The parameters common to all three examples are a uniform backward scattering map $\mathcal{B}(r) = 0.5$ and an axial tilt of $\beta = 25°$. Figures 4.1a and 4.1b correspond to a thin ring with face-on ($\hat{\mathbf{o}} = \hat{\mathbf{z}}$) and edge-on ($\hat{\mathbf{o}} = \hat{\mathbf{y}}$) observation respectively, and Fig. 4.1c shows face-on observation of a thick ring with a uniform optical depth $\tau(r) = 2$. We can make intuitive sense of these plots. As the ring system, which has a fixed orientation $\hat{\mathbf{n}}$, orbits the star, the component of its surface that faces the star is determined by $|\hat{\mathbf{n}} \cdot \hat{\mathbf{i}}| = \sin\beta |\sin\omega t|$. The factor $\sin(\omega t)$ explains why the light curve of each half-orbit is roughly sinusoidal. Deviations from this are due to the time-dependent integral $f(t)$, which in the case of a uniform albedo is proportional to the total area of $\mathcal{D}(t)$, the part of the rings that is both illuminated and visible to the observer. From the left plots of Fig. 4.1 we see that this area in minimal during equinoxes ($t = 0$ and $t = T/2$) and maximal during solstices ($t = T/4$ and $t = 3T/4$). The sharp peek seen in Fig. 4.1b is due to the shadowed and blocked parts of the ring system overlapping around $t = T/4$ for this edge-on observation, resulting in the area of $\mathcal{D}(t)$ increasing here. For face-on observation this overlap does not occur, and thus $f(t)$ is symmetric in Fig. 4.1a. The large decrease in amplitude of the second half of the light curve in Fig. 4.1c is due to the fact that for thick rings the forward and backward scattering maps are related by $\mathcal{F} = (1 - \mathcal{B}) \cdot e^{-\tau}$ as opposed to $\mathcal{F} = \mathcal{B}$ for thin rings.

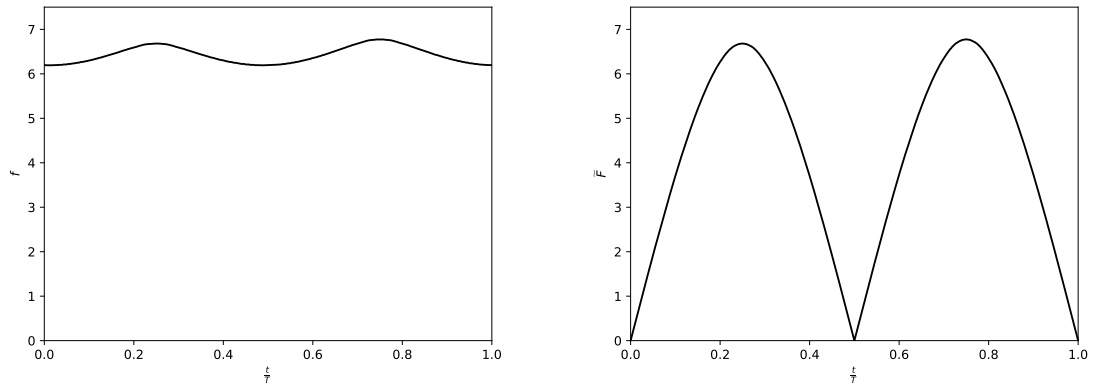

(a)

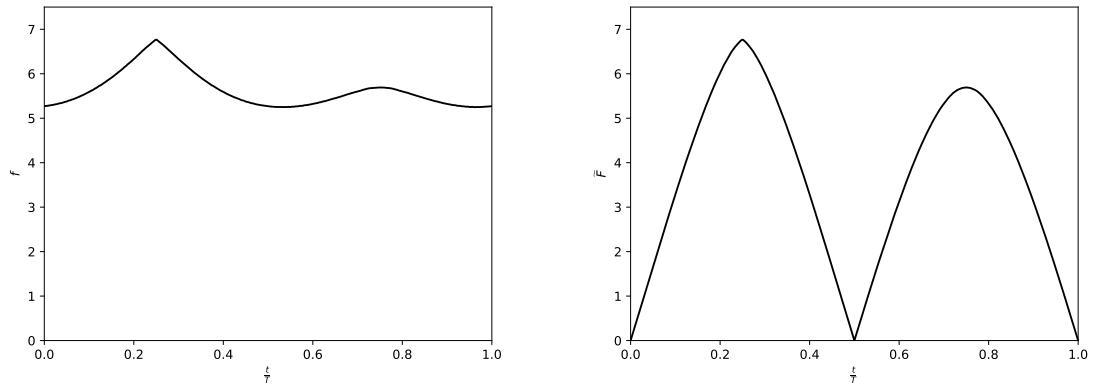

(b)

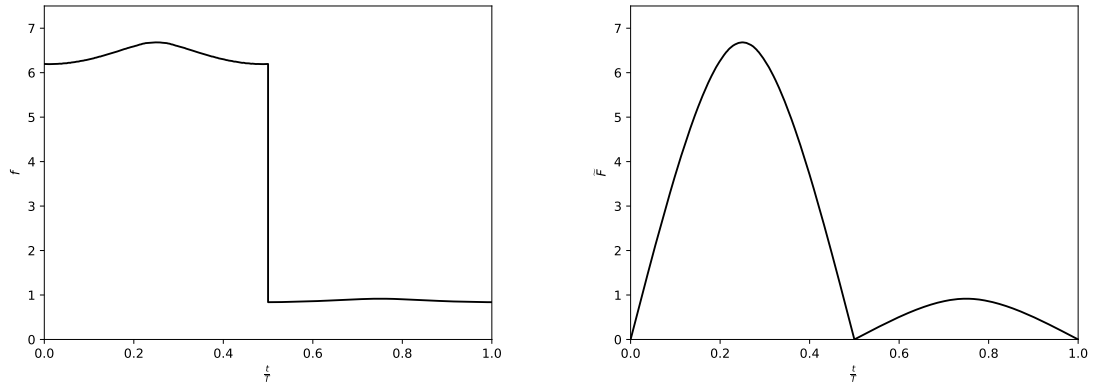

(c)

Figure 4.1: Examples of light curves of exoplanetary ring systems. The left plots show the integral $f(t)$ from Eq. (4.1), which in this case (uniform albedo) is proportional to the total area of $\mathfrak{D}(t)$, the part of the rings that is both visible and illuminated. The right plots show the corresponding light curve $\widetilde{F}(t) = |\sin(\omega t)| \cdot f(t)$, which is proportional to the observed signal $F(t)$ from Eq. (3.3). The parameters common to all three examples are $\mathcal{B}(r) = 0.5$ and $\beta = 25°$. (a) and (b) correspond to a thin ring with face-on ($\hat{\mathbf{o}} = \hat{\mathbf{z}}$) and edge-on ($\hat{\mathbf{o}} = \hat{\mathbf{y}}$) observation respectively, and (c) shows face-on observation of a thick ring with optical depth $\tau(r) = 2$.

4.3 Inverting the transformation matrix

If the transformation matrix $\mathbf{A}$ were invertible, the albedo map $\mathbf{M}$ could be retrieved by simply multiplying both sides of Eq. (4.5) by $\mathbf{A}^{-1}$ to obtain $\mathbf{M} = \mathbf{A}^{-1} \cdot \mathbf{f}$. This is not possible however, since $\mathbf{A} \in \mathbb{R}^{N_t \times N_r}$ is generally not even a square matrix. Thus a different approach is needed in order to retrieve the albedo map. We will make use of the Moore-Penrose inverse, also known as the pseudoinverse. The pseudoinverse $\mathbf{A}^+$ of a matrix $\mathbf{A}$ is a generalization of the regular inverse of a square matrix that exists and is unique for all matrices [16]. Equation (4.5) generally has multiple solutions, and the Moore-Penrose inverse can be used to select one of them. This works as follows:

For any linear map $\mathbf{A} : \mathbb{R}^{N_r} \to \mathbb{R}^{N_t}$, a vector $\mathbf{M} \in \mathbb{R}^{N_r}$ can be expressed $\mathbf{M} = \mathbf{M}_r + \mathbf{M}_n$ with $\mathbf{M}_r \in \text{Row}(\mathbf{A})$ and $\mathbf{M}_n \in \text{Null}(\mathbf{A})$. Similarly, any $\mathbf{f} \in \mathbb{R}^{N_t}$ can be expressed as $\mathbf{f} = \mathbf{f}_c + \mathbf{f}_n$ with $\mathbf{f}_c \in \text{Row}(\mathbf{A}^T) = \text{Col}(\mathbf{A})$ and $\mathbf{f}_n \in \text{Null}(\mathbf{A}^T)$. The blue arrows in Fig. 4.2 illustrate that $\mathbf{A}$ maps both $\mathbf{M}$ and $\mathbf{M}_r$ to $\mathbf{f}_c$, while $\mathbf{M}_n$ is mapped to $\mathbf{0}$. This means that if $\text{Null}(\mathbf{A}) \neq \{\mathbf{0}\}$, i.e. is $\mathbf{A}$ is not full rank, there is not a unique albedo map $\mathbf{M}$ corresponding a given light curve $\mathbf{f}$ according to $\mathbf{f} = \mathbf{A} \cdot \mathbf{M}$. There is however a one-to-one correspondence between vectors $\mathbf{f}_c \in \text{Col}(\mathbf{A})$ and $\mathbf{M}_r \in \text{Row}(\mathbf{A})$ [17]. The Moore-Penrose inverse $\mathbf{A}^+$ is the operator that makes this connection from $\mathbf{f}_c$ to $\mathbf{M}_r$. It is defined by

$$\mathbf{A}^+\mathbf{f} = \begin{cases} \mathbf{M}_r & \text{if } \mathbf{f} \in \text{Col}(\mathbf{A}) \\ \mathbf{0} & \text{if } \mathbf{f} \in \text{Null}(\mathbf{A}) \end{cases} \tag{4.8}$$

Thus, for an arbitrary $\mathbf{f} \in \mathbb{R}^{N_t}$ we have

$$\mathbf{A}^+\mathbf{f} = \mathbf{A}^+(\mathbf{f}_c + \mathbf{f}_n) = \mathbf{M}_r + \mathbf{0} = \mathbf{M}_r \tag{4.9}$$

The behavior of $\mathbf{A}^+$ is illustrated by the orange arrows in Fig. 4.2. Thus, the Moore-Penrose inverse $\mathbf{A}^+$ finds a solution $\mathbf{M}_r$ to $\mathbf{f} = \mathbf{A} \cdot \mathbf{M}$ that is unique up to the addition of an $\mathbf{M}_n \in \text{Null}(\mathbf{A})$. Furthermore, since $\text{Null}(\mathbf{A}) = \text{Row}(\mathbf{A})^\perp$, we have that for all solutions $\hat{\mathbf{M}}$

$$||\hat{\mathbf{M}}||_2 = ||\mathbf{M}_r||_2 + ||\mathbf{M}_n||_2 \geq ||\mathbf{M}_r||_2 \tag{4.10}$$

Thus, the solution $\mathbf{M}_r$ found by the Moore-Penrose inverse is the one with minimum Euclidean norm. We will call this solution the retrieved albedo map corresponding to the light curve $\mathbf{f}$.

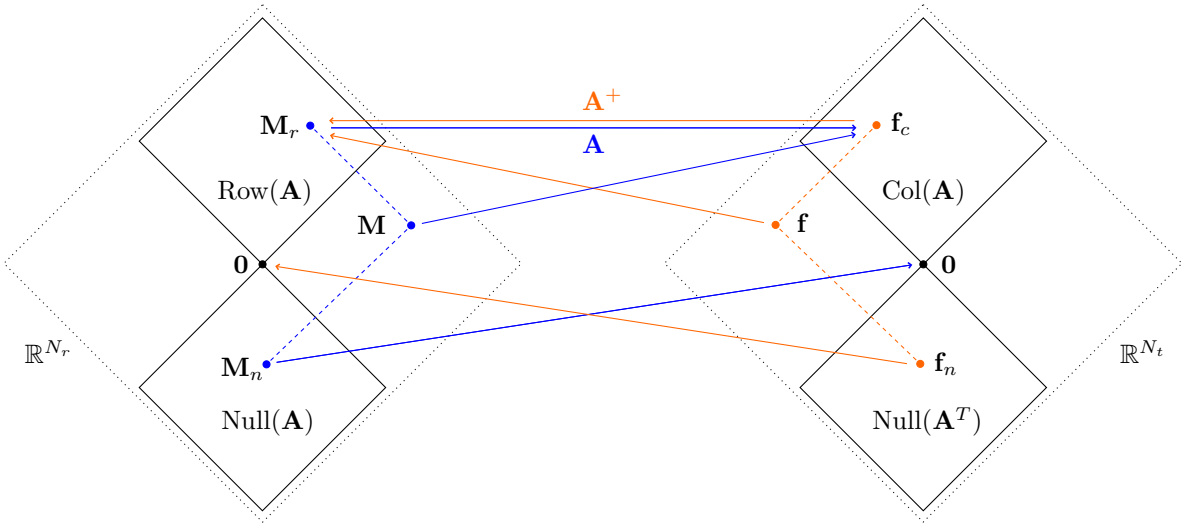

Figure 4.2: For any linear operator $\mathbf{A} : \mathbb{R}^{N_r} \to \mathbb{R}^{N_t}$, any $\mathbf{M} \in \mathbb{R}^{N_r}$ can be expressed as $\mathbf{M} = \mathbf{M}_r + \mathbf{M}_n$ with $\mathbf{M}_r \in \text{Row}(\mathbf{A})$ and $\mathbf{M}_n \in \text{Null}(\mathbf{A})$. Similarly, any $\mathbf{f} \in \mathbb{R}^{N_t}$ can be expressed as $\mathbf{f} = \mathbf{f}_c + \mathbf{f}_n$ with $\mathbf{f}_c \in \text{Row}(\mathbf{A}^T) = \text{Col}(\mathbf{A})$ and $\mathbf{f}_n \in \text{Null}(\mathbf{A}^T)$. This figure illustrates the behavior of $\mathbf{A}$ (blue arrows) and its Moore-Penrose inverse $\mathbf{A}^+$ (orange arrows) defined in Eq. (4.8).

4.4 Singular value decomposition

In Sec. 4.3 it is explained how the albedo map $\mathbf{M}_r$ can be retrieved from a given light curve $\mathbf{f}$ using the Moore-Penrose inverse $\mathbf{A}^+$ of the transformation matrix $\mathbf{A}$ in Eq. (4.5). This section will cover how $\mathbf{A}^+$ can be computed using the singular value decomposition of $\mathbf{A}$. Any $N_t \times N_r$ matrix $\mathbf{A}$ can be written as

$$\mathbf{A} = \mathbf{U}\mathbf{\Sigma}\mathbf{V}^T, \tag{4.11}$$

where $\mathbf{U}$ and $\mathbf{V}$ are respectively $N_t \times N_t$ and $N_r \times N_r$ orthogonal matrices and $\mathbf{\Sigma}$ is a $N_t \times N_r$ rectangular diagonal matrix, i.e. $\mathbf{\Sigma}_{ij} = 0$ if $i \neq j$. The diagonal entries $\sigma_i = \mathbf{\Sigma}_{ii}$ are called the singular values of $\mathbf{M}$. These are always non-negative, and the number of non-zero ones is equal to rank($\mathbf{M}$). The singular value decomposition is not unique. For the sake of convenience will assume that the σ_i are arranged in decreasing order. This makes $\mathbf{\Sigma}$ unique (but not $\mathbf{U}$ and $\mathbf{V}$). It can be shown that the pseudoinverse $\mathbf{A}^+$ of $\mathbf{A}$ is given by

$$\mathbf{A}^+ = \mathbf{V}\mathbf{\Sigma}^+\mathbf{U}^T \tag{4.12}$$

where $\mathbf{\Sigma}^+$, the pseudoinverse of $\mathbf{\Sigma}$, is formed by replacing every non-zero entry σ_i in $\mathbf{\Sigma}$ by its reciprocal and transposing the resulting matrix. There is however a problem that arises when numerically computing $\mathbf{A}^+$ is this way, which we do using the NumPy function np.linalg.pinv [18]. Numerical rounding errors can result singular values σ_i that should be zero actually getting very small positive values. These very small but non-zero singular values result in very large entries in $\mathbf{\Sigma}^+$, since their reciprocal is taken, that should have been zeros. The resulting pseudoinverse $\mathbf{A}^+$ does not map vectors $\mathbf{f} \in \text{Null}(\mathbf{A})$ to $\mathbf{0}$, as in Eq. (4.9), but to some other $\mathbf{M} \in \mathbb{R}^{N_r}$, which leads to huge errors when trying to find the retrieved albedo map $\mathbf{M}_r$. To prevent this, a singular value cutoff ratio (SVCR) is defined, and all numerically computed singular values $\sigma_i \leq \text{SVCR} \cdot \sigma_{max}$ are set to zero, where $\sigma_{max} = \sigma_1$ is the largest singular value. If a suitable value for the SVCR is used, this insures that the resulting pseudoinverse $\mathbf{A}^+$ behaves as intended. Figure 4.3 shows two examples of a singular value spectrum, in this case the spectra of the transformation matrix $\mathbf{A}$ corresponding to face-on observation ($\hat{\mathbf{o}} = \hat{\mathbf{z}}$) during the first half of the orbit ($0 \leq t \leq T/2$) with $\beta = 25°$, $N_r = N_\phi = 100$, and $N_t = 150$ for Fig. 4.3a and $N_t = 200$ for Fig. 4.3b. The horizontal line in Fig. 4.3a represents a suitable cutoff ratio of SVCR $= 10^{-10}$. Figure 4.3b shows that increasing N_t from 150 to 200 actually makes the discretization in time fine enough for $\mathbf{A}$ to become full rank, so no cutoff ratio is needed and all singular values can be included in the computation of $\mathbf{A}^+$.

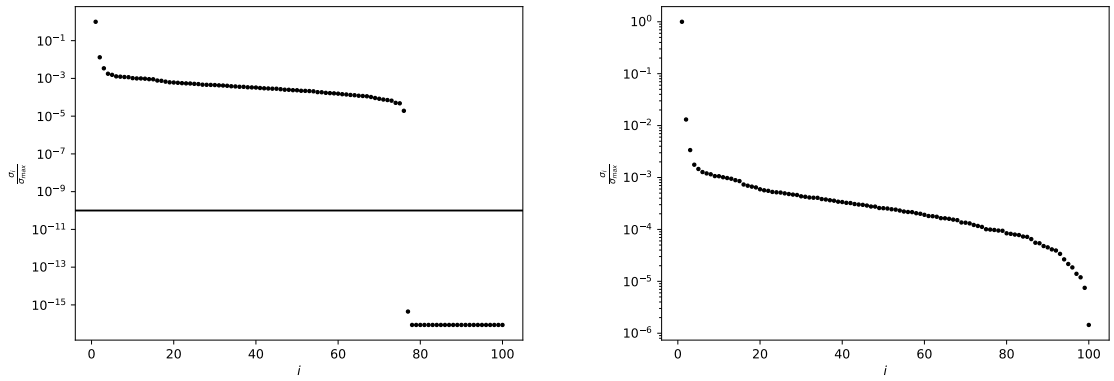

(a) (b)

Figure 4.3: Singular value spectra of the transformation matrix $\mathbf{A}$ corresponding to face-on observation ($\hat{\mathbf{o}} = \hat{\mathbf{z}}$) during the first half of the orbit ($0 \leq t \leq T/2$) with $\beta = 25°$, $N_r = N_\phi = 100$, and (a) $N_t = 150$, (b) $N_t = 200$. The horizontal line in (a) represents a suitable cutoff ratio of SVCR $= 10^{-10}$. No cutoff is needed in (b) because there $\mathbf{A}$ is full rank.

4.5 Retrieval of the optical properties of model ring systems

In this section we make use of two model backward scattering maps $\mathcal{B}(r)$; a step function map and a sinusoidal map. We also use a model optical depth map of $\tau(r) = 2$. Together, $\mathcal{B}$ and τ fix the corresponding forward scattering maps $\mathcal{F}(r)$ according to the thick ring approximation, Eq. (2.3). The corresponding light curves are calculated and the inversion process from Sec. 4.3 is then applied to retrieve the albedo maps and the optical depth. The model backward scattering maps used are given by Eqs (4.13) and (4.14). Figure 4.4 shows a grayscale image representation, where an albedo of 0 corresponds to a black surface and an albedo of 1 corresponds to a white surface.

$$\mathcal{B}_{\text{model}}(r) = \begin{cases} 0.1, & \text{if } r_p \leq r < r_p + \frac{1}{5}(r_{\text{Roche}} - r_p) \\ 0.3, & \text{if } r_p + \frac{1}{5}(r_{\text{Roche}} - r_p) \leq r < r_p + \frac{2}{5}(r_{\text{Roche}} - r_p) \\ 0.9, & \text{if } r_p + \frac{2}{5}(r_{\text{Roche}} - r_p) \leq r < r_p + \frac{3}{5}(r_{\text{Roche}} - r_p) \\ 0.6, & \text{if } r_p + \frac{3}{5}(r_{\text{Roche}} - r_p) \leq r < r_p + \frac{4}{5}(r_{\text{Roche}} - r_p) \\ 0.1, & \text{if } r_p + \frac{4}{5}(r_{\text{Roche}} - r_p) \leq r \leq r_{\text{Roche}} \end{cases} \tag{4.13}$$

$$\mathcal{B}_{\text{model}}(r) = 0.1 + 0.8 \left| \sin\left(2\pi \frac{r - r_p}{r_{\text{Roche}} - r_p} \right) \right|, \quad \text{if } r_p \leq r \leq r_{\text{Roche}} \tag{4.14}$$

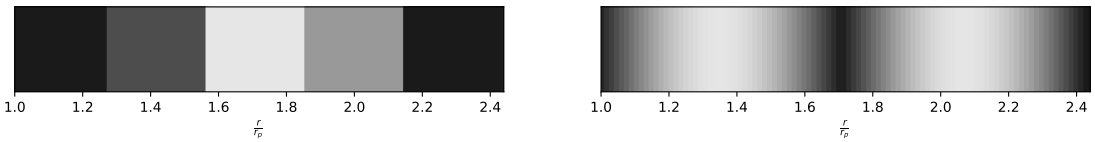

(a) (b)

Figure 4.4: Grayscale image representation of the model backward scattering maps given by (a) Eq. (4.13) and (b) Eq. (4.14). An albedo of 0 corresponds to a black surface and an albedo of 1 corresponds to a white surface.

The discretization used is $N_r = N_\phi = 100$, $N_t = 200$. The parameters that are varied are the observer position ($\hat{\mathbf{o}} = (0, 1, 0)$ (edge-on observation) and $\hat{\mathbf{o}} = (0, 0, 1)$ (face-on observation)) and the axial tilt ($\beta = 5°, 15°, 25°$). Gaussian white noise with various signal-to-noise ratios (S/N $= \infty$ (no noise), $10^4, 10^3, 10^2$) is also added to make the light curves more realistic. This noise can be thought of as a combination of instrumental noise and background noise from other celestial bodies. We will examine how much noise can be added before meaningful retrieval becomes impossible. The S/N is defined by

$$\text{S/N} = \frac{P_{\text{signal}}}{P_{\text{noise}}}, \tag{4.15}$$

where P is the average power. Because of this noise a singular value cutoff (SVCR) must be used during the inversion process, as explained in Sec. 4.4. The optimal SVCR depends on the standard deviation σ of the noise and on the dimensions of the transformation matrix $\mathbf{A}$ [19], and in this case is given by SVCR $\approx 2.798\sigma\sqrt{N_r}$. To assess the accuracy of the retrieval, the root mean square deviation (RMSD) is calculated, defined by

$$\text{RMSD} = \sqrt{\frac{1}{N_r} \sum_{n=0}^{N_r - 1} (\mathcal{B}_{\text{model}}(r_n) - \mathcal{B}_{\text{retrieved}}(r_n))^2} \tag{4.16}$$

where $\mathcal{B}$ can also be replaced by $\mathcal{F}$ or τ. The retrieved maps $\mathcal{B}(r)$ are shown in Fig. 4.5 for the step function map and Fig. 4.6 for the sinusoidal map. The thick ring approximation can be rewritten as

$$\tau(r) = \ln\left(\frac{1 - \mathcal{B}(r)}{F(r)} \right). \tag{4.17}$$

Using this, Fig. 4.7 shows the retrieved optical depth maps using both model backward scattering maps, for edge-on observation with $\beta = 25°$, with various signal-to-noise ratios (S/N $= \infty, 10^5, 10^4$).

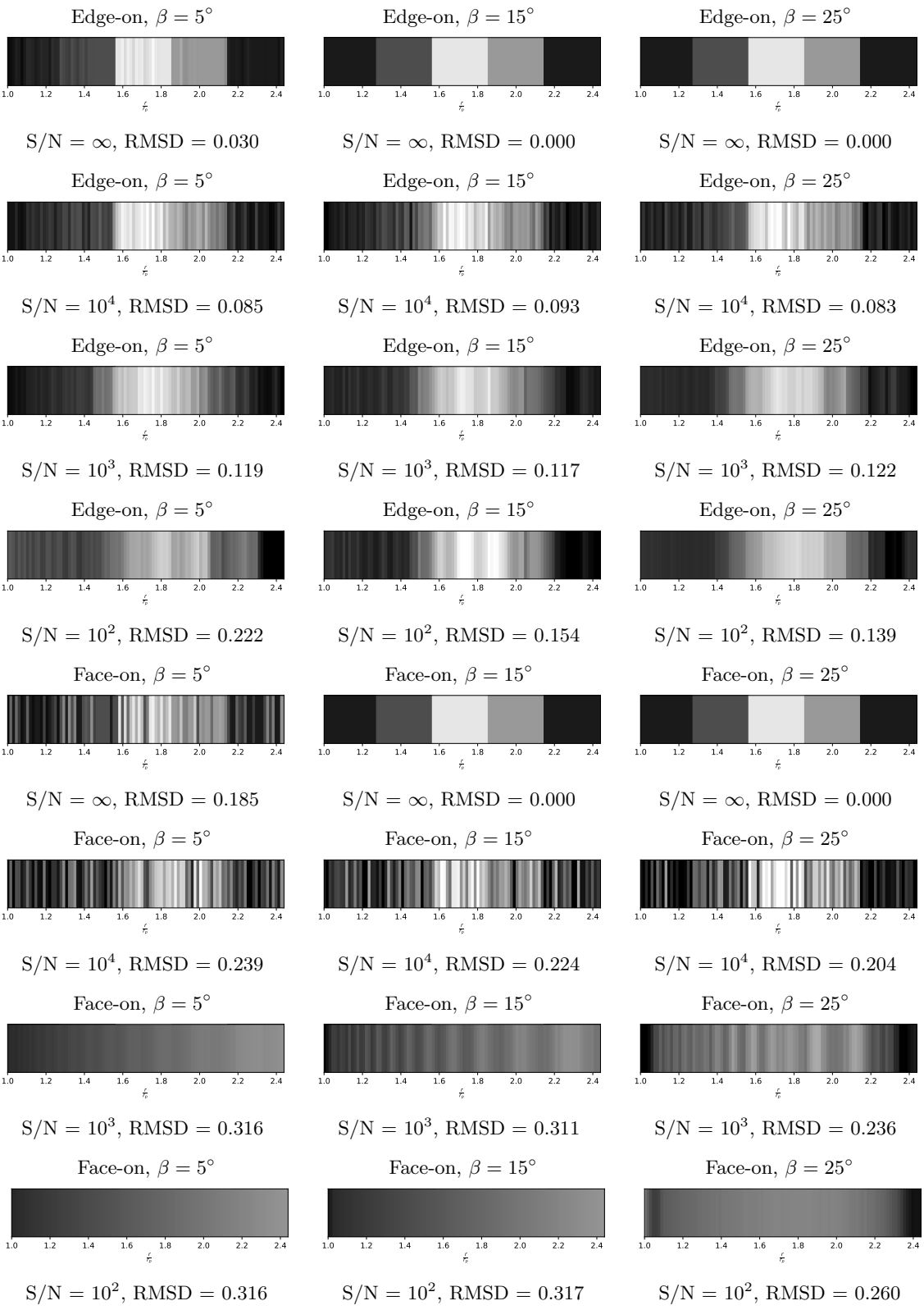

Figure 4.5: Retrieved backward scattering maps with the RMSD using the model map $\mathcal{B}(r)$ from Eq. (4.13). The discretization used is $N_r = N_\phi = 100$, $N_t = 200$. The parameters that are varied are the observer position (edge-on and face-on), the axial tilt ($\beta = 5°, 15°, 25°$), and the signal-to-noise ratio ($\text{S/N} = \infty, 10^4, 10^3, 10^2$).

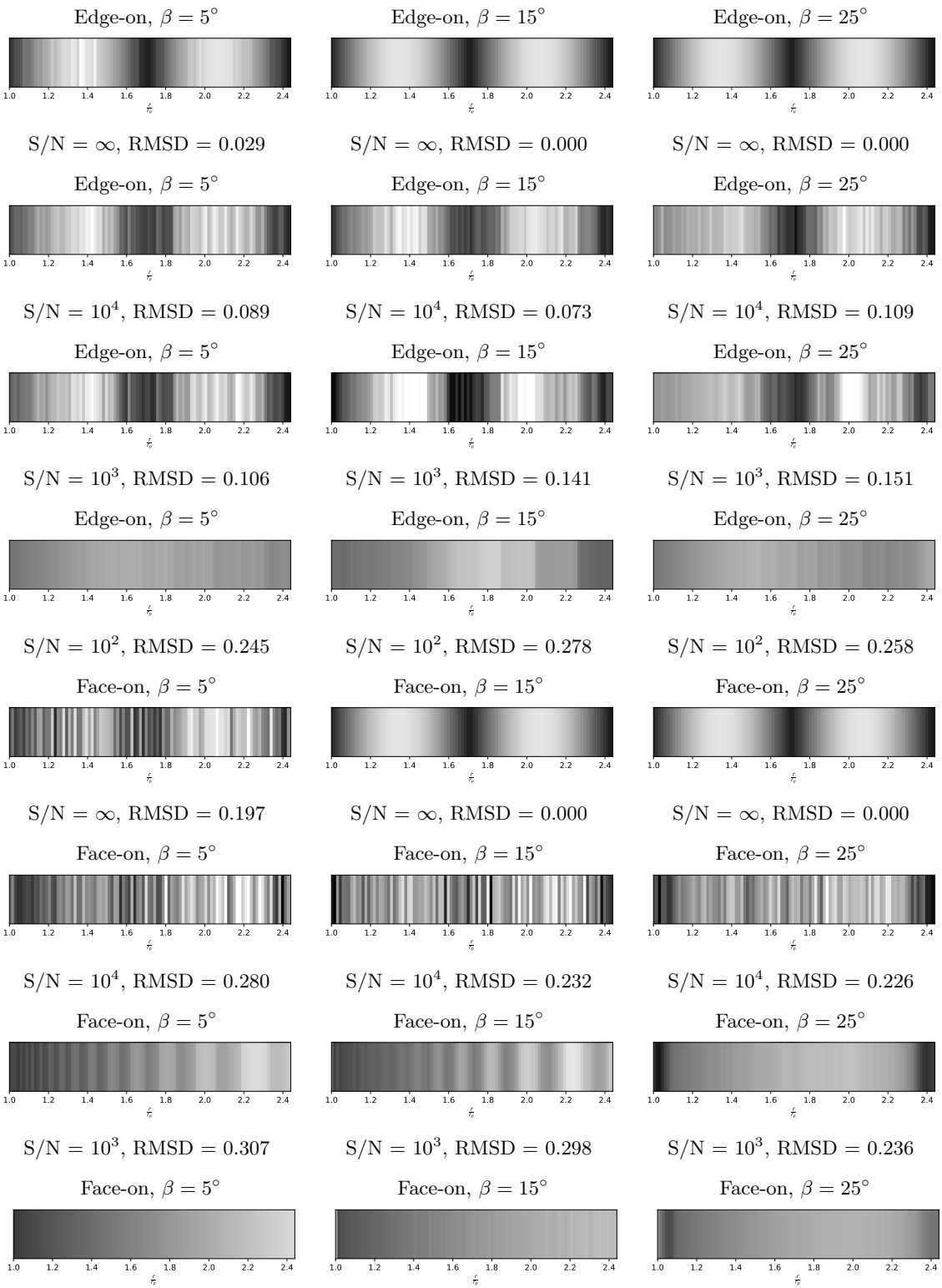

Figure 4.6: Retrieved backward scattering maps with the corresponding RMSD using the model map $\mathcal{B}(r)$ from Eq. (4.14). The discretization used is $N_r = N_\phi = 100$, $N_t = 200$. The parameters that are varied are the observer position (edge-on and face-on), the axial tilt ($\beta = 5°, 15°, 25°$), and the signal-to-noise ratio (S/N $= \infty, 10^4, 10^3, 10^2$).

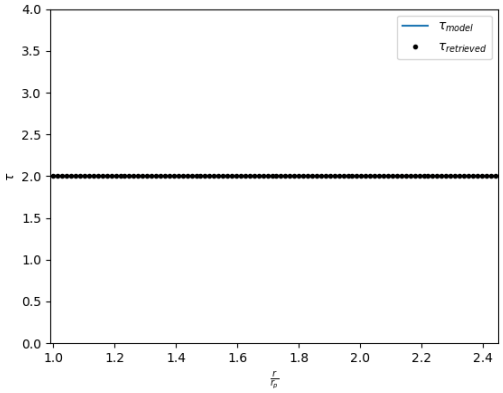

S/N $= \infty$, RMSD $= 0.000$

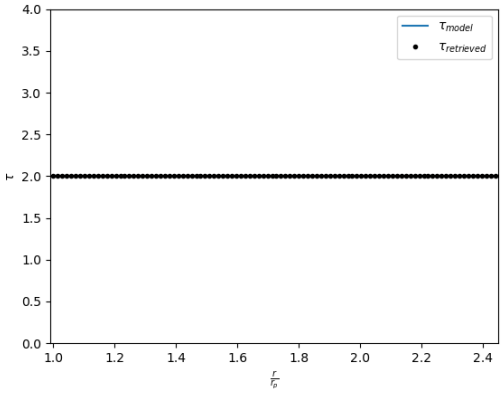

S/N $= \infty$, RMSD $= 0.000$

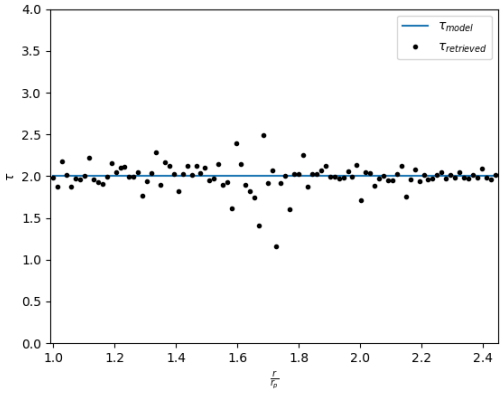

S/N $= 10^5$, RMSD $= 0.165$

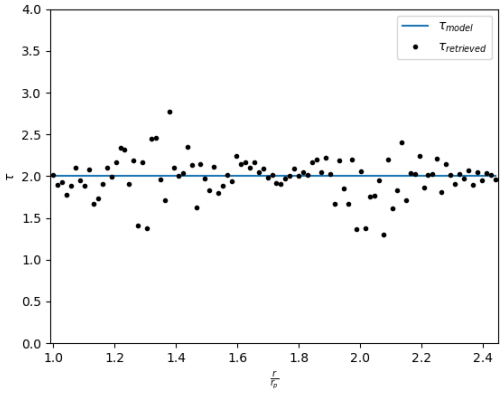

S/N $= 10^5$, RMSD $= 0.236$

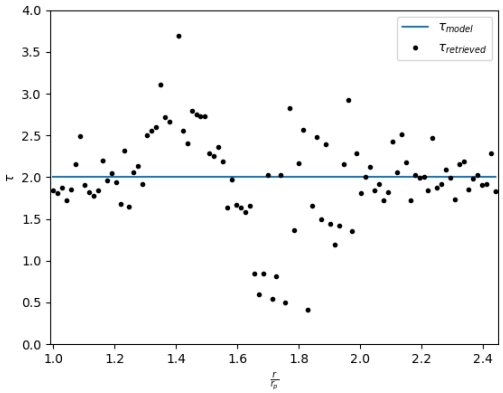

S/N $= 10^4$, RMSD $= 0.583$

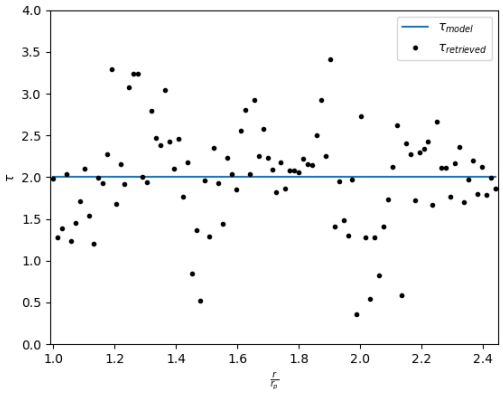

S/N $= 10^4$, RMSD $= 0.595$

Figure 4.7: Retrieved optical depth maps with the corresponding RMSD using the model map $\tau(r) = 2$. The discretization used is $N_r = N_\phi = 100$, $N_t = 200$. The axial tilt is $\beta = 25°$ and the observation is edge on. The parameters that are varied are the signal-to-noise ratio (S/N $= \infty, 10^5, 10^4$) and the backward scattering map $\mathcal{B}(r)$ (left plots: step function map (Eq. (4.13)), right plots: sinusoidal map (Eq. (4.14))).

Discussion and conclusion

In this chapter we will analyse and discuss the results from Sec. 2.2, where albedo maps of Saturn's rings were constructed and the optical depth was retrieved, and the results from Sec. 4.5, where the developed numerical inversion process was applied to retrieve the albedo maps and optical depth of model ring systems.

5.1 Optical depth of Saturn's rings

In Fig. 2.4, showing the backward and forward scattering map of Saturn, we see that the general profile of the two maps is similar, and that many of the peaks in one map can also be identified in the other, indicating that in the construction of the maps they were properly aligned. We must also mention that there is one point, at around $\frac{r}{r_p} = 2.05$, where the two graphs exactly touch, i.e. $\mathcal{B} = \mathcal{F}$, and that at the very right of the plot, we see that $\mathcal{B} + \mathcal{F} = 1$ exactly. This happens because of the way the maps were normalized in order to make them physically sensible, as explained in Sec. 2.2, and does not necessarily reflect the actual relation between the two albedo maps of Saturn's rings at these points. In Fig. 2.5, which shows the optical depth, the drop-off to zero at the right end also happens because of this, since at this point $\mathcal{B} + \mathcal{F} = 1$, so that $\tau(r) = \ln((1 - \mathcal{B})/F) = 0$. We can compare Fig. 2.5 with existing literature about the optical depth of Saturn's rings, derived from an occultation of the star γ Crusis observed by Cassini's visible and infrared mapping spectrometer (VIMS) [20]. For the C ring, the optical depth ranges from 0.05 to 0.12, which does not agree with our results. This is not surprising however, since the thick ring approximation, from which τ is calculated, is not at all accurate for such small values of τ. For the B-ring, the optical depth varies from 0.4 to greater than 5. This does match well with our findings: in our figure the optical depth is at around 0.5 at $r/r_p = 1.6$, and exceeds 5 around $r/r_p = 1.8$. For the A ring, the optical depth is between 0.4 and 0.9. Our results show slightly more variation, with values mostly between 0.0 and 1.2, with one spike of 2.4. This indicates that at in this regime the thick ring approximation is not extremly accurate, but does have some explanatory power.

5.2 Albedo map and optical depth retrieval of model rings

The are a number of patterns visible in Figs 4.5 and 4.6 that can be explained, both in the grayscale plots as well as in the RSMDs. First of all, the retrieval is perfect if no noise is added to the light curve, except for the smallest axial tilt of $\beta = 5°$, where there is a non-zero RMSD. Overall we observe that the error tends to increase as β decreases. If the signal-to-noise ratio decreases, the error invariably goes up, as is of course expected. At the smallest S/N of 10^2, the retrieved map in some cases still looks somewhat similar to the model map, but in others it looks nothing like the model and is completely useless. We also see that the retrieval tends to be better for edge-on observation than for face-on observation. This is likely due to the fact that for edge-on observation, there is a part of the planet's orbit where the shadowed and blocked parts of the ring system overlap, as explained in Sec. 4.2. This overlapping affects the light curves of the each of the individual ringlets differently (depending on their radius), and thus creates more variation in the total light curve, making it easier to recover the albedo map. Finally, the accuracy of the retrieval is approximately the same for both of the model backward scattering maps used. In Fig. 4.7 we see that if no noise is added, the retrieval of the optical depth is perfect. However, the error quickly increases as the signal-to-noise ratio is increased, and the retrieval is very poor even for a relatively large S/N of 10^4.

5.3 Conclusion

As next-generation telescopes will be able to directly measure the light curves of exoplanets, methods of analyzing this data must be developed so we can expand our knowledge of planetary systems both in the Solar System and in the rest of the universe. This thesis has demonstrated the potential of using light curve analysis for the retrieval of the albedo map and optical depth of exoplanetary ring systems. We developed a mathematical model for how light interacts with ring particles through absorption, transmission, and scattering, and derived an analytic formula for the light curve of a ring system. This formula was then translated into a numerical linear transformation linking albedo map to light curve. Through the use of the Moore-Penrose pseudoinverse and singular value decomposition, the process was inverted to retrieve albedo maps from light curves.

The validity of this method was tested on synthetic data from model ring systems. The results showed that under favorable conditions, in particular high signal-to-noise ratios and edge-on observation, the retrieval process can accurately reconstruct the albedo map and optical depth. Under less favorable conditions the accuracy of the retrieval significantly decreases and eventually becomes entirely useless. The model was also used to analyse Saturn's rings. The retrieved optical depth based on albedo maps constructed from high-resolution images from NASA's Cassini space probe generally agrees with existing literature, particularly for the optically dense B ring, where the thick ring approximation is valid. However, the results were not accurate for the C ring, where the model's assumptions are less applicable due to the sparsity of this ring.

Some recommendations for future research are the development of a more general model for the reflection properties of a planetary ring system that encompasses both the thick and thin ring approximation used in this thesis, and including the light curve of the planet in the analysis by combining our model with similar light-reflection models analysing the light curves of exoplanets, so as to create a more complete framework for analysing planetary systems using light curves.

Bibliography

[1] A. Wolszczan and D. A. Frail. A planetary system around the millisecond pulsar psr1257 + 12. *Nature*, 1992.

[2] NASA Exoplanet Archive (2023) – processed by Our World in Data. "Cumulative number of exoplanets discovered" [dataset]. NASA Exoplanet Archive (2023) [original data].

[3] N. B. Cowan and E. Agol. Inverting phase functions to map exoplanets. *The Astrophysical Journal*, 678(2), 2008.

[4] N. B. Cowan and Y. Fujii. Mapping exoplanets. *Handbook of Exoplanets*, pages 1–18, 2021.

[5] B. Farr, W. M. Farr, N. B. Cowan, H. M. Haggard, and T. Robinson. A bayesian framework for mapping exoplanets in reflected light. *The Astronomical Journal*, 156(4):146, 2018.

[6] H. Kawahara and Y. Fujii. Global mapping of earth-like exoplanets from scattered light curves. *The Astrophysical Journal*, 720(2):1333–1350, 2010.

[7] S.N. Stuger. Exoplanet surface mapping using scattered light curves, 2021. [Bachelor's thesis, TU Delft]. TUD repository.

[8] NASA/JPL/Space Science Institute. http://photojournal.jpl.nasa.gov/catalog/PIA08389. Public Domain.

[9] NASA / JPL / Space Science Institute. http://photojournal.jpl.nasa.gov/catalog/PIA07874. Public Domain.

[10] J. N. Winn and M. J. Holman. The transit light curve project. ix. evidence for a smaller radius of the exoplanet xo-3b. *The Astrophysical Journal*, 683(2):1076–1084, 2008.

[11] A. Palazzolo. Formalism for the rotation matrix of rotations about an arbitrary axis. *Am. J. Phys*, 44(1):63–67, 1976.

[12] Mike Luciuk. Roche Limit: Why Do Comets Break Up? https://web.archive.org/web/20130515200347/http://www.asterism.org/tutorials/tut25-1.htm.

[13] Michael A. Zeilik and Stephan A. Gregory. *Introductory Astronomy & Astrophysics (4th ed.)*. Saunders College Publishing, 1998.

[14] Australia Telescope National Facility. Luminosity of stars. https://web.archive.org/web/20140809144429/http://www.atnf.csiro.au/outreach//education/senior/astrophysics/photometry_luminosity.html.

[15] A. M. Chwatal and G. R. Raidl. *Determining Orbital Elements of Extrasolar Planets by Evolution Strategies*. Springer Berlin Heidelberg, 2007. pages 870-877.

[16] G. H. Golub and C. F. Van Loan. *Matrix computations (3rd ed.)*. Baltimore: Johns Hopkins, 1996. pages 257-258.

[17] G. Strang. *Linear algebra and its applications*. Thomson, 2006. Section 3.1.

[18] NumPy Developers. https://numpy.org/doc/stable/reference/generated/numpy.linalg.pinv.html.

[19] Matan Gavish and David L. Donoho. The optimal hard threshold for singular values is 4/sqrt(3). https://arxiv.org/abs/1305.5870, 2014.

[20] M.M. Hedman and P.D. Nicholson. The b-ring's surface mass density from hidden density waves: Less than meets the eye? *Icarus*, 279:109–124, 2016.

Appendix

6.1 Source code

```
# Imports

import numpy as np
import matplotlib.pyplot as plt
from mpl_toolkits.mplot3d import Axes3D
import matplotlib.image as img

get_ipython().run_line_magic('matplotlib', 'widget')

# Define parameters

r_p = 5.8232e7 # Planet radius (m)
beta = np.pi/180*25 # Planet and ring axil tilt angle (rad)
o = [0,1,0] # Observer direction
omega = 6.765314061e-9 # Angular frequency of planet orbit (rad/s)

N_r = 50 # Number of ring radius sample points
N_phi = 50 # Number of ring angle sample points
N_t = 100  # Number of sample points in time in a half orbit

SNratio = 1e5 # Signal-to-noise ratio
noiseOn = False # Turn noise on and of

thick = True # True, False for thick, thin ring approximation respectively

# Backward scattering map of the ring
def B(r):
    if r < r_p + 0.2*1.44*r_p:
        m = 0.1
    elif r < r_p + 0.4*1.44*r_p:
        m = 0.3
    elif r < r_p + 0.6*1.44*r_p:
        m = 0.9
    elif r < r_p + 0.8*1.44*r_p:
        m = 0.6
    else:
        m = 0.1
    return m

# Optical depth of the ring
def tau(r):
    return 2

# Forward scattering map of the ring
def F(r):
    if thick == True:
        return (1-B(r))*np.exp(-tau(r))
    else:
        return B(r)

T = 2*np.pi/omega # Orbit period (s)
R = 1.434e9 # Orbital radius (m)
n_hat = np.sin(beta)*np.array([0,1,0]) + np.cos(beta)*np.array([0,0,1]) # Unit planet
    and ring rotation axis
o_hat = o/np.sqrt(np.dot(o,o)) # Unit observer axis
sign = omega*np.dot(n_hat,o_hat) # If sign>0 backward scattered light can reach the
    observer for the first half of
                                 # the orbit, and forward scattered for the second
    half. If sign<0 it's the other way around.
```

```
                                # (If sign=0, the signal is zero.)

# Make a visual of the planet and ring

fig = plt.figure()
ax = fig.add_subplot(111, projection='3d')

# Planet
draw_planet = False
if draw_planet:
    u, v = np.mgrid[0:2*np.pi:100j, 0:np.pi:50j]
    x = np.cos(u)*np.sin(v)
    y = np.sin(u)*np.sin(v)*np.cos(beta) - np.cos(v)*np.sin(beta)
    z = np.sin(u)*np.sin(v)*np.sin(beta) + np.cos(v)*np.cos(beta)
    ax.plot_wireframe(x/2.44,y/2.44,z/2.44, color='blue', linewidth=4)

# Ring
for r in np.linspace(r_p,2.44*r_p,100):
    rho,phi = np.mgrid[r:r:1j, 0:2*np.pi:50j]
    x = np.cos(phi)
    y = np.sin(phi)*np.cos(beta)
    z = np.sin(phi)*np.sin(beta)
    color = str(B(r))
    ax.plot_wireframe(x*rho/(2.44*r_p),y*rho/(2.44*r_p),z*rho/(2.44*r_p), color=color
    )

ax.set_xlim([-1,1])
ax.set_ylim([-1,1])
ax.set_zlim([-1,1])
ax.set_xlabel('x')
ax.set_ylabel('y')
ax.set_zlabel('z')
plt.show()

# Define what the ring looks like (in multiple useful ways)

# Returns the matrix for a rotation around axis with angle theta (in radians).
def rotation_matrix(axis, theta):
    unit_axis = axis/np.sqrt(np.dot(axis,axis))
    x,y,z = unit_axis
    s,c = np.sin(theta),np.cos(theta)
    return np.array([[c + x*x*(1-c)  , x*y*(1-c) - z*s, x*z*(1-c) + y*s],
                     [y*x*(1-c) + z*s, c + y*y*(1-c)  , y*z*(1-c) - x*s],
                     [z*x*(1-c) - y*s, z*y*(1-c) + x*s, c + z*z*(1-c)  ]])

# Define points on the ring by indeces n_r and n_phi
rIndices = range(N_r)
phiInices= range(N_phi)
S_index = []
for r in rIndices:
    for phi in phiInices:
        S_index.append([r,phi])

# Define the ring in the xy-plane: S
S = []
for s in S_index:
    r = r_p*(1+1.44*s[0]/(N_r-1))
    phi = 2*np.pi/N_phi*s[1]
    S.append([r*np.cos(phi),r*np.sin(phi),0])

# Define the ring with the correct orientation in the chosen coordinate system:
    S_beta
S_beta = []
for s in S:
    S_beta.append(np.matmul(rotation_matrix([1,0,0],-beta),s))

# Define what the ring looks like when looking at it from the observer's point of
    view: S_o
x_hat = [1,0,0]
chi = np.cross(x_hat,o_hat)
zeta = -np.arccos(np.dot(x_hat,o_hat))
```

```
125
126 if np.array_equal(chi,[0,0,0]): # To deal with the case that o_hat//x_hat
127     chi = [0,0,1]
128     if np.dot(x_hat,o_hat) == 1:
129         zeta = 0
130     else:
131         zeta = np.pi
132
133 S_o = []
134 for s in S_beta:
135     S_o.append(np.matmul(rotation_matrix(chi,zeta),s))
136
137 # Define what the ring looks like at time t when looking at it from the star's point
      of view: S_s(t)
138 def getS_s(t):
139     S_s = []
140     for s in S_beta:
141         S_s.append(np.matmul(rotation_matrix([0,0,1],-omega*t),s))
142     return S_s
143
144 # Numerically calculate the transformation matrices and the interegral part f of the
      light curve F of the ring system
145
146 dr = 1.44*r_p/(N_r-1)
147 dphi = 2*np.pi/N_phi
148 drdphi = dr*dphi
149 ts = np.linspace(0,T/2,N_t) # Times at which we measure
150
151 # Values of f at the measured times
152 fs1 = np.zeros(N_t)
153 fs2 = np.zeros(N_t)
154 # Numerical transformation matrix for both halves of orbit
155 A1 = np.zeros((N_t,N_r))
156 A2 = np.zeros((N_t,N_r))
157
158 for n_t, t in enumerate(ts):
159     S_s1 = getS_s(t)
160     S_s2 = getS_s(t + T/2)
161     f_t1 = 0
162     f_t2 = 0
163     for i, s in enumerate(S_index):
164         if S_o[i][0] > 0 or np.sqrt(S_o[i][1]**2 + S_o[i][2]**2) > r_p: # Check if
      visible to observer
165             if S_s1[i][0] > 0 or np.sqrt(S_s1[i][1]**2 + S_s1[i][2]**2) > r_p: #
      Check if illuminated
166                 r = r_p*(1+1.44*s[0]/(N_r-1))
167                 ds2 = r*drdphi
168                 A1[n_t][s[0]] += ds2
169                 if sign > 0:
170                     f_t1 += B(r)*ds2
171                 else:
172                     f_t1 += F(r)*ds2
173             if S_s2[i][0] > 0 or np.sqrt(S_s2[i][1]**2 + S_s2[i][2]**2) > r_p: #
      Check if illuminated
174                 r = r_p*(1+1.44*s[0]/(N_r-1))
175                 ds2 = r*drdphi
176                 A2[n_t][s[0]] += ds2
177                 if sign > 0:
178                     f_t2 += F(r)*ds2
179                 else:
180                     f_t2 += B(r)*ds2
181     fs1[n_t] = f_t1
182     fs2[n_t] = f_t2
183
184 As = [A1,A2]
185 fs1, fs2 = np.array(fs1), np.array(fs2)
186 fss = [fs1, fs2]
187
188 # Add Gaussian white noise to f
189 if noiseOn:
190     sd1 = np.mean(fs1)/(SNratio*np.sqrt(2/np.pi))
```

```
    sd2 = np.mean(fs2)/(SNratio*np.sqrt(2/np.pi))
    fs1 = fs1 + np.random.normal(0,sd1,len(fs1))
    fs2 = fs2 + np.random.normal(0,sd2,len(fs2))

# Plot the integral f
fs = np.concatenate((fs1,fs2))
plt.figure()
plt.plot(np.concatenate((ts,ts+T/2))/T,fs,'k')
plt.xlabel('fractT')
plt.ylabel('f')
plt.xlim((0,1))
plt.show()

# Calculate the light curve F
Fss = []
for i in range(2):
    Fs = np.dot(n_hat,o_hat)/(2*np.pi*R**2)*np.sin(beta)*abs(np.sin(omega*(ts+i*T/2))
    )*fss[i]
    Fss.append(Fs)

# Plot F
Fs = np.concatenate((Fss[0],Fss[1]))
plt.figure()
plt.plot(np.concatenate((ts,ts+T/2))/T,Fs,'k')
plt.xlabel('fractT')
plt.ylabel('F')
plt.xlim((0,1))
plt.show()

# Plot RMSD as a function of the number of singular values included

rmsdss = []
OptNumOfSs = []
Sings = []
for i, A in enumerate(As):
    U,Sing,Vh = np.linalg.svd(A)
    Sings.append(Sing)
    rmsds = []
    for j in range(len(Sing)):
        if j == len(Sing)-1:
            rcond = (Sing[-1]/2)/Sing[0]
        else:
            rcond = Sing[j+1]/Sing[0]
        A_plus = np.linalg.pinv(A,rcond)
        M_recs = np.matmul(A_plus,fss[i])
        sd = 0
        for n_r, M_rec in enumerate(M_recs):
            if sign > 0:
                if i == 0:
                    sd += (M_rec - B(r_p*(1+1.44*n_r/(N_r-1))))**2
                else:
                    sd += (M_rec - F(r_p*(1+1.44*n_r/(N_r-1))))**2
            else:
                if i == 0:
                    sd += (M_rec - F(r_p*(1+1.44*n_r/(N_r-1))))**2
                else:
                    sd += (M_rec - B(r_p*(1+1.44*n_r/(N_r-1))))**2

        rmsds.append(np.sqrt(sd/N_r))
    rmsdss.append(rmsds)

    OptNumOfS = rmsds.index(np.min(rmsds)) + 1
    OptNumOfSs.append(OptNumOfS)

xs = np.linspace(1,N_r,N_r)
plt.figure()
plt.plot(xs,rmsdss[0],'k.',ms=5, label='1st half of orbit: optimal #σ = ' + str(
    OptNumOfSs[0]) + ', RMSD = '
                                        + str(np.around(rmsdss[0][OptNumOfSs[0]-1],4)
    ))
plt.plot(xs,rmsdss[1],'.',ms=5, label='2nd half of orbit: optimal #σ = ' + str(
```

```
    OptNumOfSs[1]) + ', RMSD = '
                                        + str(np.around(rmsdss[1][OptNumOfSs[1]-1],4)
    ))
plt.xlabel('#σ included')
plt.ylabel('RMSD')
plt.legend()
plt.show()

# Plot the retrieved maps B and F (visual of the ring)

rs = []
for n_r in rIndices:
    rs.append(r_p*(1+1.44*n_r/(N_r-1)))
rs = np.array(rs)

B_gens, F_gens = [], []

for r in rs:
    B_gens.append(B(r))
    F_gens.append(F(r))

M_recss = []
rconds = []
for i in range(2):
    if OptNumOfSs[i] == N_r:
        rcond = (Sings[i][-1]/2)/Sings[i][0]
    else:
        rcond = Sings[i][OptNumOfSs[i]]/Sings[i][0]
    rconds.append(rcond)
    A_plus = np.linalg.pinv(As[i],rcond)
    M_recs = np.matmul(A_plus,fss[i])
    M_recss.append(M_recs)

fig = plt.figure()
ax = fig.add_subplot(1, 1, 1)

for n_r, r in enumerate(rs):
    if M_recss[0][n_r] > 1:
        color = '1'
    elif M_recss[0][n_r] < 0:
        color = '0'
    else:
        color = str(M_recss[0][n_r])
    plt.vlines(r/r_p,0,1,color,linewidth=10)
    if sign >= 0:
        B_recs = M_recss[0]
        F_recs = M_recss[1]
        plt.vlines(r/r_p,1,2,str(B_gens[n_r]),linewidth=10)
        plt.yticks((0.5,1.5),('$\mathcal{B}_{retrieved}$','$\mathcal{B}_{generated}$'))
    else:
        plt.vlines(r/r_p,1,2,str(F_gens[n_r]),linewidth=10)
        plt.yticks((0.5,1.5),('$\mathcal{F}_{retrieved}$','$\mathcal{F}_{generated}$'))

plt.axhline(1)
plt.xlabel('$fracrr_p$')
plt.xlim(1,2.44)
plt.ylim(0,2)
plt.gca().set_aspect(0.25)
plt.show()

fig = plt.figure()
ax = fig.add_subplot(1, 1, 1)

for n_r, r in enumerate(rs):
    if M_recss[1][n_r] > 1:
        color = '1'
    elif M_recss[1][n_r] < 0:
        color = '0'
    else:
        color = str(M_recss[1][n_r])
    plt.vlines(r/r_p,0,1,color,linewidth=10)
```

```
    if sign < 0:
        plt.vlines(r/r_p,1,2,str(B_gens[n_r]),linewidth=10)
        plt.yticks((0.5,1.5),('$\mathcal{B}_{retrieved}$','$\mathcal{B}_{generated}$'))
    else:
        plt.vlines(r/r_p,1,2,str(F_gens[n_r]),linewidth=10)
        plt.yticks((0.5,1.5),('$\mathcal{F}_{retrieved}$','$\mathcal{F}_{generated}$'))

plt.axhline(1)
plt.xlabel('$fracrr_p$')
plt.xlim(1,2.44)
plt.ylim(0,2)
plt.gca().set_aspect(0.25)
plt.show()

# Plot the recoverd maps (as a function)

plt.figure()
plt.plot(rs/r_p,B_gens)
plt.plot(rs/r_p,B_recs,'k.',ms=4)
plt.xlim(1,2.44)
plt.xlabel('$fracrr_p$')
plt.ylabel('$\mathcal{B}$')
plt.title('Backward scattering')
plt.show()

plt.figure()
plt.plot(rs/r_p,F_gens)
plt.plot(rs/r_p,F_recs,'k.',ms=4)
plt.xlim(1,2.44)
plt.xlabel('$fracrr_p$')
plt.ylabel('$\mathcal{F}$')
plt.title('Forward scattering')
plt.show()

# Plot the singular value spectrum of the transformation matrix

xs = np.linspace(1,N_r,N_r)

plt.figure()
plt.yscale('log')
plt.plot(xs,Sings[0]/Sings[0][0],'k.',ms=5, label='First half of orbit')
plt.axhline(rconds[0],color='k',label='SVCR 1 = ' + str(np.around(rconds[0],6)))
plt.plot(xs,Sings[1]/Sings[1][0],'.',ms=5, label='Second half of orbit')
plt.axhline(rconds[1],label='SVCR 2 = ' + str(np.around(rconds[1],6)))
plt.xlabel('$i$')
plt.ylabel('$frac\sigma_i\sigma_{max}$')
plt.legend()
plt.show()

# Recover optical depth

tau_gens = []
for r in rs:
    tau_gens.append(tau(r))

tau_recs = []
for i in range(N_r):
    tau_recs.append(np.log((1-B_recs[i])/F_recs[i]))

plt.figure()
plt.plot(rs/r_p,tau_gens, label='$tau_{model}$')
plt.plot(rs/r_p, tau_recs,'k.',label='$tau_{retrieved}$')
plt.xlim((0.99,2.45))
plt.ylim((0,4))
plt.xlabel('$fracrr_p$')
plt.ylabel('$tau$')
plt.legend()
plt.show()

# Read scattering maps of Saturn's rings
bsm = img.imread('Saturn backward scattering map 200 points.jpg')
```

```
fsm = img.imread('Saturn forward scattering map 200 points.jpg')

# Define B and F for Saturn
B_S = []
for i in range(len(fsm[0])):
    B_S.append(np.sum(bsm[0][int(i/len(fsm[0])*len(bsm[0]))]))
B_S = np.array(B_S)/np.max(B_S)

F_S = []
for i in range(len(fsm[0])):
    F_S.append(np.sum(fsm[0][i]))
F_S = F_S/np.max(F_S)

# Make sure F <= B is satisfied
maxRatio = 0
for i in range(len(B_S)):
    if F_S[i]/B_S[i] > maxRatio:
        maxRatio =  F_S[i]/B_S[i]
F_S = F_S/maxRatio

# Make sure F + B <= 1 is satifsied
maxi = 0
for i in range(len(B_S)):
    if B_S[i] + F_S[i] > maxi:
        maxi = B_S[i] + F_S[i]
B_S, F_S = B_S/maxi, F_S/maxi

# Plot B and F for Saturn
r_Saturn = 58232 # Radius of Saturn (km)
xs = np.linspace(74500,136780,len(fsm[0]))/r_Saturn

plt.figure()
plt.plot(xs,B_S,'k',label='$\mathcal{B}$')
plt.plot(xs,F_S,label='$\mathcal{F}$')
plt.xlabel('$fracrr_p$')
plt.ylabel('$\mathcal{M}$')
plt.legend()
plt.xlim(np.min(xs),np.max(xs))
plt.show()

# Plot tau for Saturn
tau = np.log((1-B_S)/F_S)

plt.figure()
plt.plot(xs,tau,'k')
plt.xlim(min(xs),max(xs))
plt.xlabel('$fracrr_p$')
plt.ylabel('$tau$')
plt.show()
```